International Journal of Solids and Structures xxx (2014) xxx–xxx

Contents lists available at ScienceDirect

International Journal of Solids and Structures

journal homepage: www.elsevier.com/locate/ijsolstr

Low-energy impact response of composite and sandwich composite plates with piezoelectric sensory layers

Theofanis S. Plagianakos *, Evangelos G. Papadopoulos

National Technical University of Athens, Department of Mechanical Engineering, Control Systems Laboratory, Athens GR-15780, Greece

ARTICLE INFO

Article history:
Received 17 November 2013
Received in revised form 8 March 2014
Available online xxxx

Keywords:
Low-energy impact
Piezoelectric
Composite
Sandwich
Plates
Layerwise mechanics
Interfacial stress

ABSTRACT

An efficient model reduction based methodology is presented for predicting the global (impact force, plate deflection and electric potential) and through-thickness local (interfacial strains and stresses) dynamic response of pristine simply-supported cross-ply composite and sandwich composite plates with piezoelectric sensory layers subjected to low-energy impact. The through-thickness response of the laminate is modelled using coupled higher-order layerwise displacement-based piezoelectric laminate theories. Linearized contact laws are implemented for simulating the impactor–target interaction during impact. The stiffness, mass, piezoelectric and permittivity matrices of the plate are formulated from ply to structural level and reduced by applying a Guyan reduction technique to yield the structural system in state space. This reduction technique enables the formulation of a plate–impactor structural system of minimum size (1 term per vibration mode for composite plates – 2 terms for sandwich plates) and reduces computational cost, thus facilitating applicability for real-time impact and vibration control.

1. Introduction

The dynamic response of composite and sandwich composite plates under low-energy impact is of practical significance in automotive, aerospace and every-day life applications, in cases such as a tool drop during repair, a hit by a runaway stone or the fall of a composite cell-phone case from a table to the floor, where the damage caused may be invisible, while the inclusion of piezoelectric sensory layers into the lamination enables monitoring of the structural response on-site in real-time. The prediction of the global and local through-thickness impact response of such smart structures is essential during the design phase in order to determine the impact force, the type and duration of impact, to estimate stresses at the interface between composite and piezoelectric material layers and to quantify the signals acquired by the piezoelectric layers. These predictions, combined with a computationally efficient plate–impactor system model, are expected to contribute to the development of appropriate algorithms for active impact control and control for energy harvesting.

The importance of the impact response of composite and sandwich composite structures is highlighted by the amount of work conducted in this field so far. Extensive related literature reviews have been conducted among others by Cantwell and Morton (1991), Abrate (1997, 1998, 2001), Qiu and Yu (2011) and Chai and Zhu (2011), while relevant papers have been reported by Stronge (2000) in his book on impact mechanics. On the basis of the kinematic assumptions used to predict the response of the impacted composite or sandwich composite structure, the existing models may be divided into two main categories: (i) mass–spring models without (Shivakumar et al., 1985; Wu and Yu, 2001; Olsson, 2002; Zhou and Stronge, 2006) or with dampers (Olsson, 2003; Anderson, 2005) and (ii) full continuum models based on energy equilibrium equations. The latter may encompass exact, analytical or finite element solutions and can potentially predict the impact response in several positions of the structure, including all displacements, strains and stresses. Moreover, depending on the amount of the vibration modes taken into account, continuum models can capture multiple impacts caused by the induced vibration triggered by the impact event. Analytical solutions for composite plates subjected to low-velocity impacts have been developed among others by Christoforou and Swanson (1991), and Christoforou and Yigit (1998), on the basis of Kirchhoff's plate theory kinematics and a linearized elasto-plastic contact law between the plate and impactor (Yigit and Christoforou, 1994), whereas Chun and Lam (1998) implemented Reddy's higher-order single layer plate theory and a Hertzian contact law. Finite element solutions for predicting the low-velocity impact response of composite plates have been reported among others by Sun and Chen (1985), who developed a quadratic Lagrange element based on Reissner–Mindlin kinematics and an experimentally determined non-linear indentation law, Wu and Chang (1989), who formulated

* Corresponding author. Tel.: +30 210 7722348; fax: +30 210 7721455.
E-mail address: fanplag@gmail.com (T.S. Plagianakos).

http://dx.doi.org/10.1016/j.ijsolstr.2014.04.005
0020-7683/

a 3-D plate theory and a corresponding brick element to study out of plane stresses in addition to plate deflection and contact force, and Choi and Chang (1992), who predicted damage due to impact and reported relevant experimental results. As far as sandwich plates subjected to low-velocity impact are concerned, Palazotto et al. (2000) formulated a C^2-continuous finite element based on higher-order single-layer kinematics and geometrical nonlinearity for conducting progressive failure analysis, whereas Besant et al. (2001) combined first order shear shell elements for the faces with brick elements for the core, considered elastoplastic material behaviour and degradation, and reported numerical and experimental results. Yang and Qiao (2005) developed an analytical solution based on a higher-order laminate theory and predicted global (contact force and deflection) and local through-thickness (propagation of normal and shear stresses) response, and predicted failure locations, time and modes in sandwich composite beams. Icardi and Ferrero (2009) reported a refined plate element based on global-local 3-D layerwise kinematic assumptions, considered material degradation and predicted damage and through-thickness distributions of transverse displacement and interlaminar shear stress, in addition to temporal variation of the contact force. A Ritz-type solution based on 3-D higher-order single-layer mixed kinematics was developed by Malekzadeh et al. (2006) for predicting the dynamic response of sandwich plates subjected to multiple impacts. Analytical and finite element solutions were also reported by Hoo Fatt and Park (2001) and Kärger et al. (2008), respectively. Experimental results for composite and sandwich composite plates subjected to low-velocity impact were reported among others by Sjöblom et al. (1988), Lee et al. (1993), Ambur et al. (1995), Hazizan and Cantwell (2002), Schubel et al. (2005), Christoforou et al. (2010) and Yang et al. (2013). The idea of embedding piezoelectric sensors to composite structures in order to detect impact location and reconstruct the contact force time-profile was reported in the late 90's by Tracy and Chang (1998) and Seydel and Chang (2001), and has been elaborated for the design of real-time monitoring networks (Park et al., 2009; Liu and Chattopadhyay, 2013). The active control of impact response of composite plates and shells by means of piezoelectric layers and patches towards the minimization of contact force has been studied by Saravanos and Christoforou (2002a,b), who developed an analytical solution based on first-order shear kinematics for the composite laminate and a linear layerwise approximation of electric potential. Yet, the local through-thickness impact response of sandwich piezoelectric composite plates in the case of low-velocity and low-energy impact has not been studied so far. Moreover, in the vast majority of existing work employing full continuum models for predicting impact response of composite or sandwich plates, the full plate–impactor system is solved. This leads to large matrix sizes and increased computational effort for detailed through-thickness modelling, such as in the case of layerwise laminate theories.

In this paper, an efficient Ritz-type solution is presented, which is based on higher-order layerwise through-thickness kinematic assumptions and a Guyan reduction technique, for predicting both global (plate deflection, contact force and electric potential) and local (through-thickness distribution of displacements, strains and stresses) response of pristine simply-supported cross-ply composite and sandwich composite plates with piezoelectric layers subjected to low-energy impact. In the proposed method, the full structural system containing all Fourier modal displacement amplitudes is reduced to one containing a single deflection amplitude per mode, leading to dramatic savings in size and computational effort, which is a most useful capability for real-time control applications. Still, the information included in the full structural system is retained and recovered after solving the reduced system by expressing the dependent modal variables and their derivatives via the modal deflection of the plate. The accuracy of the proposed method is validated by comparisons with published numerical results for composite plates without/with piezoelectric layers and with experimental results for sandwich composite plates.

2. Theoretical formulation

In this section, the integrated theoretical framework developed for simulating the impact response of a sandwich composite plate with piezoelectric layers subjected to low-energy impact is developed, starting from a general composite material ply with piezoelectric properties and arriving to the solution of the structural system in state-space.

2.1. Formulation of plate-subsystem structural matrices

2.1.1. Basic physical assumptions

The theoretical framework developed is based on the following assumptions:

- The impact energy is low, such as no material damage is induced by the impact event.
- The impact is elastic, thus, there is no loss of energy in the form of heat.
- The laminate plies are perfectly bonded together throughout the impact event.

2.1.2. Governing material equations

In general, the laminate layers including the piezoelectric, composite and foam plies are assumed to exhibit linear piezoelectric behaviour. In the following formulation, displacements and electric potential and all other variables arising from these (strains, stresses, etc.) are time-dependent. The ply constitutive equations in the natural coordinate system Oxyz (Fig. 1(a)) have the form:

$$\begin{aligned} \boldsymbol{\sigma}_i &= C_{ij}^{E}\mathbf{S}_j - (e_{mi})^{T}\mathbf{E}_m \\ \mathbf{D}_m &= e_{mj}\mathbf{S}_j + \varepsilon_{mm}^{S}\mathbf{E}_m \end{aligned} \tag{1}$$

where $i, j = 1,\ldots,6$ and $m = 1,\ldots,3$; $\boldsymbol{\sigma}_i$ and $\mathbf{S}_j$ are the mechanical stress and engineering strain, respectively, in vectorial notation; $\mathbf{E}_m$ is the electric field vector; $\mathbf{D}_m$ is the electric displacement vector; C_{ij} is the elastic stiffness tensor; e_{mj} is the piezoelectric tensor arising from the piezoelectric charge tensor and the stiffness tensor; and ε_{mm} is the electric permittivity tensor of the material. The form of the above tensors is shown in Appendix A. Superscripts E and S indicate a constant electric field, and strain conditions, respectively. The above equations may encompass the behaviour of both an off-axis homogenized fibrous piezoelectric ply and a passive composite ply ($e_{mj} = 0$). The electric field vector E_m is the gradient of the electric potential $\boldsymbol{\varphi}$ along basis vectors x, y, z of the natural coordinate system:

$$\mathbf{E}_m = -\partial\boldsymbol{\varphi}_m/\partial\mathbf{x}_m \tag{2}$$

In the current work, piezoelectric components polarized through-thickness are considered.

2.1.3. Through-thickness kinematic assumptions

A typical composite or sandwich composite laminate with piezoelectric components is subdivided into n discrete layers as shown schematically in Fig. 1(a). Each discrete-layer may contain either a single ply, a sub-laminate, or a sub-ply. In the case of composite plates, the displacement field assumed through the thickness of the laminate is based on a 2-D higher-order layerwise formulation (HLPT 2-D – Plagianakos and Saravanos, 2008), which approximates displacements and electric potential by piecewise linear, parabolic and cubic functions of the discrete layer thickness (Fig. 1(b)), while maintaining displacement continuity across

Please cite this article in press as: Plagianakos, T.S., Papadopoulos, E.G. Low-energy impact response of composite and sandwich composite plates with piezoelectric sensory layers. Int. J. Solids Struct. (2014), http://dx.doi.org/10.1016/j.ijsolstr.2014.04.005

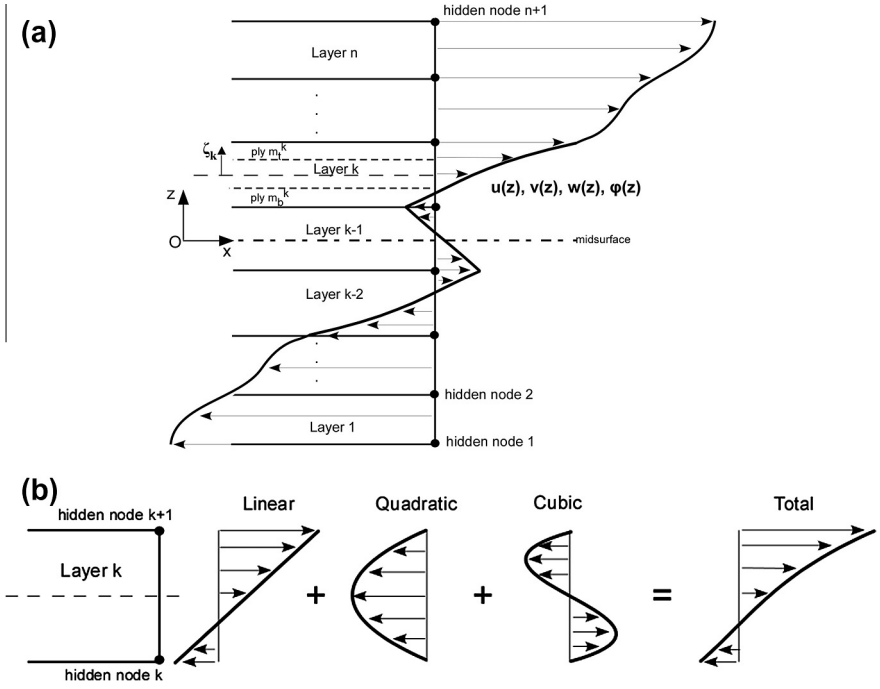

Fig. 1. Typical sandwich piezoelectric composite laminate configuration analyzed with n-discrete layers. (a) Discrete layers with natural coordinate system and local thickness coordinate ζ_k used for predicting arbitrary distribution of displacements and electric potential through the laminate thickness; (b) assumed displacement and electric potential components through the thickness of a discrete layer.

discrete layer boundaries. For the sandwich structures, the core compressibility effects are taken into account by applying a similar through-thickness approximation on the transverse displacement (HLPT 3-D). In this context, the kinematic assumptions take the form:

Both composite and sandwich plates

$$\begin{aligned}\mathbf{u}^k(x,y,\zeta_k) &= U^k(x,y)\Psi_1^k(\zeta_k) + U^{k+1}(x,y)\Psi_2^k(\zeta_k) + \alpha_x^k(x,y)\Psi_3^k(\zeta_k) + \lambda_x^k(x,y)\Psi_4^k(\zeta_k)\\ \mathbf{v}^k(x,y,\zeta_k) &= V^k(x,y)\Psi_1^k(\zeta_k) + V^{k+1}(x,y)\Psi_2^k(\zeta_k) + \alpha_y^k(x,y)\Psi_3^k(\zeta_k) + \lambda_y^k(x,y)\Psi_4^k(\zeta_k)\\ \boldsymbol{\varphi}_z(x,y,\zeta_k) &= \Phi_z^k(x,y)\Psi_1^k(\zeta_k) + \Phi_z^{k+1}(x,y)\Psi_2^k(\zeta_k) + \alpha_\varphi^k(x,y)\Psi_3^k(\zeta_k) + \lambda_\varphi^k(x,y)\Psi_4^k(\zeta_k)\end{aligned} \tag{3}$$

Composite plates (HLPT 2-D)

$$\mathbf{w}^k(x,y,\zeta_k) = w^0(x,y)$$

Sandwich plates (HLPT 3-D)

$$\begin{aligned}\mathbf{w}^k(x,y,\zeta_k) = {} & W^k(x,y)\Psi_1^k(\zeta_k) + W^{k+1}(x,y)\Psi_2^k(\zeta_k) + \alpha_z^k(x,y)\Psi_3^k(\zeta_k)\\ & + \lambda_z^k(x,y)\Psi_4^k(\zeta_k)\end{aligned}$$

where $\mathbf{u}$ and $\mathbf{v}$ are the in-plane displacements, $\mathbf{w}$ is the transverse displacement, superscript $k = 1,\ldots,n$ denote discrete layer, and ζ_k is the local thickness coordinate of layer k defined such that $\zeta_k = 0$ at the middle of the discrete layer, $\zeta_k = 1$ and $\zeta_k = -1$ at the top and the bottom, of the discrete layer k, respectively. Ψ_1^k, Ψ_2^k are linear and Ψ_3^k, Ψ_4^k are quadratic, cubic interpolation functions, respectively, through the thickness of the layer (Appendix A). U^k, V^k, W^k, U^{k+1}, V^{k+1}, W^{k+1} and Φ_z^k, Φ_z^{k+1} are displacements and electric potential at the bottom and top of the discrete layer k, effectively describing extension and rotation, and electric potential at the terminals, respectively, of the layer, and w^0 is transverse displacement at the midplane. The terms $\alpha_x^k, \alpha_y^k, \alpha_z^k, \alpha_\varphi^k, \lambda_x^k, \lambda_y^k, \lambda_z^k, \lambda_\varphi^k$ are amplitudes of quadratic (α) and cubic (λ) variations of displacements (subscript x, y and z) and electric potential (subscript φ) through the thickness of the discrete layer. The contributions of these higher-order variations to the in-plane displacement and electric potential distribution through the thickness of the discrete layer vanish at its top and bottom interfaces.

The impact mechanics methodology is presented in the following sections for the case of constant transverse displacement through the thickness of the laminate (HLPT 2-D), whereas its application is similar for through-thickness variable transverse displacement (HLPT 3-D) and relevant modifications are reported wherever necessary.

2.1.4. Laminate energy

The stiffness and mass matrices of the sandwich composite plate are derived on the basis of Hamilton's principle,

$$\int_{t_1}^{t_2}\left(-\int_{A_o}\delta H_L dA - \int_{A_o}\delta W_{d_L} dA + \int_{A_o}\delta K_L dA + \int_\Gamma (\delta\overline{\mathbf{u}})^T\bar{\boldsymbol{\tau}} d\Gamma\right)dt = 0 \tag{4}$$

where A_0 denotes the midplane (Fig. 1(a)), $\delta\overline{\mathbf{u}}$ is the vector of all degrees of freedom of the laminate arising from the kinematic assumptions (3), $\bar{\boldsymbol{\tau}}$ are the tractions at the boundary surface Γ, δH_L and δK_L are the variations of the electromechanical and kinetic energy of the laminate per unit area, and δW_{d_L} is the variation of the dissipated energy of the laminate per unit area. The present paper focuses on the prediction of plate response during impacts for impact durations in the range of milliseconds. By taking also into account that the structural damping of the materials studied is low (Plagianakos and Saravanos, 2009), the effect of damping during impact is considered minimal and is therefore neglected.

The variations of electromechanical and kinetic energy per unit area in a composite laminate consisting of n discrete layers are expressed as:

$$\delta H_L = \sum_{k=1}^{n}\int_z \left((\delta\mathbf{S}_i^k)^T\boldsymbol{\sigma}_i - (\delta\mathbf{E}_j^k)^T\mathbf{D}_j\right)dz \tag{5}$$

$$\delta K_L = \sum_{k=1}^{n}\int_z \frac{1}{2}\left((\delta\dot{\underline{\mathbf{u}}}^k)^T\rho^k\dot{\underline{\mathbf{u}}}^k\right)dz \tag{6}$$

where k denotes discrete layer, $i = 1, 2, 4, 5, 6$ and $j = 1, 2, 3$, and $\mathbf{S}_i^k, \underline{\mathbf{u}}^k$ are mechanical strain (Appendix A) and displacement vectors.

Please cite this article in press as: Plagianakos, T.S., Papadopoulos, E.G. Low-energy impact response of composite and sandwich composite plates with piezoelectric sensory layers. Int. J. Solids Struct. (2014), http://dx.doi.org/10.1016/j.ijsolstr.2014.04.005

Combining the constitutive equations (1), the kinematic assumptions (3) and the field-potential relation (2) with Eqs. (5) and (6), and taking into account interlaminar shear stress compatibility conditions (Appendix A), the laminate energies per unit area take the form:

$$\delta H_L = \sum_{k=1}^{n}\Big[(\delta \boldsymbol{S}^k)^T[\mathbf{Q}^k]\boldsymbol{S}^k + (\delta \boldsymbol{S}_s^k)^T[\mathbf{Q}_s^k]\boldsymbol{S}_s^k - (\delta \boldsymbol{S}^k)^T[\mathbf{Q}_e^k]\mathbf{E}_3^k - (\delta \mathbf{E}_3^k)^T[\mathbf{Q}_e^k]^T\boldsymbol{S}^k - (\delta \mathbf{E}_3^k)^T[\mathbf{L}_e^k]\mathbf{E}_3^k\Big] \tag{7}$$

$$\delta K_L = \frac{1}{2}\sum_{k=1}^{n}\Big[(\delta \dot{\underline{\mathbf{u}}}^k)^T[\widehat{\mathbf{M}}^k]\dot{\underline{\mathbf{u}}}^k\Big] \tag{8}$$

where indices s and e denote the interlaminar shear strain and electric field, respectively, the overhat indicates discrete layer inertia matrix and variables in italics denote vectors reduced by imposition of interlaminar shear stress compatibility. The generalized displacement, strain and electric field vectors are given by

$$\begin{aligned}
&\dot{\underline{\mathbf{u}}}^k = \{\dot{U}^k, \dot{U}^{k+1}, \dot{V}^k, \dot{V}^{k+1}, \dot{w}^0, \dot{\alpha}_x^l, \dot{\alpha}_y^l\}\\
&\boldsymbol{S}^k = \{U_{,x}^k, U_{,x}^{k+1}, V_{,y}^k, V_{,y}^{k+1}, U_{,y}^k, U_{,y}^{k+1}, V_{,x}^k, V_{,x}^{k+1}, \alpha_{x,x}^l, \alpha_{y,y}^l, \alpha_{x,y}^l, \alpha_{y,x}^l\} \quad k=1,\ldots,n\\
&\boldsymbol{S}_s^k = \{w_{,y}^0, V^k, V^{k+1}, w_{,x}^0, U^k, U^{k+1}, \alpha_y^l, \alpha_x^l\} \quad l=1,\ldots,n-1\\
&\mathbf{E}_3^k = \{\Phi_z^k, \Phi_z^{k+1}, \alpha_\varphi^k, \lambda_\varphi^k\}
\end{aligned} \tag{9}$$

In Eq. (7), Q and Q_s are the laminate in-plane and interlaminar shear stiffness matrices, respectively, Q_e is the piezoelectric matrix and L_e is the electric permittivity matrix. These matrices include the integration through the thickness of the composite laminate and their formulation has been extensively described elsewhere (Plagianakos and Saravanos, 2008, 2009). The major benefits arising from the explicit imposition of the interlaminar shear stress compatibility include prediction of stresses at interfaces between discrete layers and the elimination of $2n+2$ independent kinematic variables by expressing the higher-order displacement terms λ^k ($k=1,\ldots,n$) and α^n as a function of the remaining ones (Appendix A). In the case of transverse compressibility (HLPT 3-D), no stress compatibility is imposed, and the displacement and strain vectors of Eq. (9) contain linear and higher-order terms of transverse displacement and their derivatives, while the out of plane normal strain is also considered.

2.1.5. In-plane approximation of elastic and electric variables

Before proceeding with integration along the plate's midsurface, as dictated by Eq. (4), an in-plane approximation of displacements and electric potential of the laminate should be implemented. In the case of a Navier solution applicable to simply-supported cross-ply composite plates with n piezoelectric layers, the electromechanical variables are approximated using a Fourier series expansion as:

$$\begin{aligned}
w^0(x,y,t) &= \sum_m\sum_n w_{mn}^0(t)\sin\left(\tfrac{m\pi}{L_x}x\right)\sin\left(\tfrac{n\pi}{L_y}y\right)\\
U^k(x,y,t) &= \sum_m\sum_n U_{mn}^k(t)\cos\left(\tfrac{m\pi}{L_x}x\right)\sin\left(\tfrac{n\pi}{L_y}y\right)\\
V^k(x,y,t) &= \sum_m\sum_n V_{mn}^k(t)\sin\left(\tfrac{m\pi}{L_x}x\right)\cos\left(\tfrac{n\pi}{L_y}y\right)\\
\alpha_x^l(x,y,t) &= \sum_m\sum_n \alpha_{x_{mn}}^l(t)\cos\left(\tfrac{m\pi}{L_x}x\right)\sin\left(\tfrac{n\pi}{L_y}y\right) \quad k=1,\ldots,n+1\\
\alpha_y^l(x,y,t) &= \sum_m\sum_n \alpha_{y_{mn}}^l(t)\sin\left(\tfrac{m\pi}{L_x}x\right)\cos\left(\tfrac{n\pi}{L_y}y\right) \quad l=1,\ldots,n-1\\
\Phi_z^k(x,y,t) &= \sum_m\sum_n \Phi_{z_{mn}}^k(t)\sin\left(\tfrac{m\pi}{L_x}x\right)\sin\left(\tfrac{n\pi}{L_y}y\right) \quad s=1,\ldots,n\\
\alpha_\varphi^s(x,y,t) &= \sum_m\sum_n \alpha_{\varphi_{mn}}^s(t)\sin\left(\tfrac{m\pi}{L_x}x\right)\sin\left(\tfrac{n\pi}{L_y}y\right)\\
\lambda_\varphi^s(x,y,t) &= \sum_m\sum_n \lambda_{\varphi_{mn}}^s(t)\sin\left(\tfrac{m\pi}{L_x}x\right)\sin\left(\tfrac{n\pi}{L_y}y\right)
\end{aligned} \tag{10}$$

With m, n mode numbers.

In the case of the HLPT 3-D, the Fourier series expansion is implemented in a similar manner for approximating the additional out of plane normal terms w^k, α_z^s, λ_z^s ($s=1,\ldots,n$), and the in-plane terms λ_x^s, λ_y^s, α_x^n, α_y^n which are not eliminated by imposition of stress compatibility.

2.1.6. Plate modal structural matrices

Substituting the expressions for laminate electromechanical and kinetic energy (7) and (8) into the governing equations of motion (4) and taking into account equations (9) and (10) the plate structural subsystem in discrete form is built for each mode pair mn:

$$\begin{bmatrix}[M_{uu}]_{mn} & 0\\ 0 & 0\end{bmatrix}\begin{Bmatrix}\ddot{\overline{\mathbf{u}}}_{mn}\\ \ddot{\overline{\boldsymbol{\varphi}}}_{mn}^P\end{Bmatrix} + \begin{bmatrix}[K_{uu}]_{mn} & [K_{u\varphi}^{PP}]_{mn}\\ [K_{\varphi u}^{PP}]_{mn} & [K_{\varphi\varphi}^{PP}]_{mn}\end{bmatrix}\begin{Bmatrix}\overline{\mathbf{u}}_{\mathbf{mn}}\\ \overline{\boldsymbol{\varphi}}_{mn}^P\end{Bmatrix} = \begin{Bmatrix}\mathbf{q}_{mn}(t) - [K_{u\varphi}^{PA}]_{mn}\overline{\boldsymbol{\varphi}}_{mn}^A\\ \mathbf{D}_{mn}^P(t) - [K_{\varphi\varphi}^{PA}]_{mn}\overline{\boldsymbol{\varphi}}_{mn}^A\end{Bmatrix} \tag{11}$$

where superscripts P and A denote passive (sensory) and active piezoelectric layers (Saravanos and Heyliger, 1995), and

$$\begin{aligned}
\overline{\mathbf{u}}_{mn} &= \left\{w_{mn}^0, U_{mn}^k, V_{mn}^k, \alpha_{x_{mn}}^l, \alpha_{y_{mn}}^l\right\}^T \quad k=1,\ldots,n+1\\
\overline{\boldsymbol{\varphi}}_{mn}^P &= \left(\left\{\Phi_{z_{mn}}^k, \alpha_{\varphi_{mn}}^s, \lambda_{\varphi_{mn}}^s\right\}^P\right)^T \quad \begin{matrix}l=1,\ldots,n-1\\ s=1,\ldots,n\end{matrix}
\end{aligned} \tag{12}$$

are the plate elastic and electric variable vectors, respectively. The vector $\mathbf{q}$ contains the externally applied loads per unit area, while $\mathbf{D}$ is the vector of externally applied charges. In the absence of external charge sources, the structural subsystem is condensed by solving the second equation of the structural subsystem for sensory electric potential vector and substituting in the first one. Thus, the electrically condensed plate subsystem takes the form:

$$[M_{uu}]_{mn}\ddot{\overline{\mathbf{u}}}_{mn} + [K_{cu}]_{mn}\overline{\mathbf{u}}_{mn} = \mathbf{q}_{mn}(t) + [K_{ce}^A]_{mn}\overline{\boldsymbol{\varphi}}_{mn}^A \tag{13}$$

where

$$\begin{aligned}
[K_{cu}]_{mn} &= [K_{uu}]_{mn} - [K_{u\varphi}^{PP}]_{mn}[K_{\varphi\varphi}^{PP}]_{mn}^{-1}[K_{u\varphi}^{PP}]_{mn}^T\\
[K_{ce}^A]_{mn} &= [K_{u\varphi}^{PP}]_{mn}[K_{\varphi\varphi}^{PP}]_{mn}^{-1}[K_{\varphi\varphi}^{PA}]_{mn} - [K_{u\varphi}^{PA}]_{mn}
\end{aligned} \tag{14}$$

In the case of the HLPT 3-D, the elastic variables' vector of Eq. (12) contains linear and higher-order terms of transverse displacement, as well as, additional in-plane higher order terms, which are eliminated by stress compatibility in the case of the HLPT 2-D.

2.1.7. Reduction of modal matrices

As indicated by Eqs. (12) and (13), the size of the mass and stiffness matrices of the plate depend on the through-thickness discretization. For a plate discretized through-thickness by n discrete layers, Eq. (12) yields $4n+1$ independent elastic variables per mode pair, thus the plate has $4n+1$ degrees of freedom (DOF), which determine the size of the mass and stiffness matrix in Eq. (13). Considering that for predicting the dynamic response of a plate subjected to a point impact the plate–impactor system should be solved for a large amount of mode pairs at each time step, the layerwise through-thickness discretization would lead to mass and stiffness matrices of large size and respective computational cost. In order to reduce this cost and enable implementation of the methodology to real-time control applications, while retaining the information regarding the through-thickness response, appropriate reduction techniques should be applied on the plate subsystem of Eq. (13). In the current formulation, a Guyan reduction scheme (Guyan, 1965; Avitabile, 2005) was adopted for being a static condensation yielding easily an expression of the plate's selected primary (independent) DOF as a function of the reduced ones, while

Please cite this article in press as: Plagianakos, T.S., Papadopoulos, E.G. Low-energy impact response of composite and sandwich composite plates with piezoelectric sensory layers. Int. J. Solids Struct. (2014), http://dx.doi.org/10.1016/j.ijsolstr.2014.04.005

other reduction techniques could be also applied. Since the impact force is assumed to act purely in the z-direction (Fig. 1(a)) and thus bending vibration modes are primarily excited, the transverse displacement was selected as the independent DOF:

$$\bar{\mathbf{u}}_{mn} = \begin{Bmatrix} w^0_{mn} \\ U^k_{mn} \\ V^k_{mn} \\ \alpha^l_{x_{mn}} \\ \alpha^l_{y_{mn}} \end{Bmatrix} = \begin{Bmatrix} \bar{\mathbf{u}}^i_{mn} \\ \bar{\mathbf{u}}^d_{mn} \end{Bmatrix} = \mathbf{T}_{mn}\bar{\mathbf{u}}^i_{mn} = \mathbf{T}_{mn} w^0_{mn} \tag{15}$$

where $\mathbf{T}_{mn}$ is the modal transformation vector, which arises from consideration of a static load case for independent (superscript i) and dependent (superscript d) elastic variables:

$$\begin{bmatrix} [K_{ii}]_{mn} & [K_{id}]_{mn} \\ [K_{di}]_{mn} & [K_{dd}]_{mn} \end{bmatrix} \begin{Bmatrix} \bar{\mathbf{u}}^i_{mn} \\ \bar{\mathbf{u}}^d_{mn} \end{Bmatrix} = \begin{Bmatrix} q^i_{mn} \\ 0 \end{Bmatrix} \tag{16}$$

$$\mathbf{T}_{mn} = \begin{Bmatrix} 1 \\ -[K_{dd}]^{-1}_{mn}[K_{di}] \end{Bmatrix} \tag{17}$$

In this context, the plate stiffness matrix for each mode pair mn is reduced as:

$$K^r_{mn} = \mathbf{T}^T_{mn}[K_{cu}]_{mn}\mathbf{T}_{mn} \tag{18}$$

The mass matrix is reduced in a similar manner:

$$M^r_{mn} = \mathbf{\Lambda}^T_{mn}[M_{uu}]_{mn}\mathbf{\Lambda}_{mn} \tag{19}$$

where $\Lambda = \{1,0,\ldots,0\}$. The implementation of the Guyan reduction includes the construction of a modal transformation vector (Eq. (17)) and of modal matrices (Eqs. (18) and (19)) statically, i.e. once for each mode pair. The corresponding computational effort is imperceptible with respect to the corresponding effort required for solving at each time step an at least five times larger system (in the case of a single discrete layer), such as the full plate-impactor system. On the other hand, due to the static nature of the Guyan reduction technique, the mass is underestimated for an increasing mode number (Qu, 2004). However, as illustrated in Section 3, mass underestimation results to deviations of a few percent between predictions of the full and reduced system natural frequencies. This deviation has very small significance compared to the benefit gained by the system size reduction in terms of computational efficiency.

The plate matrices reduction procedure yields per mode pair mn a single term for stiffness and mass, respectively. These terms represent the modal stiffness and inertia properties of the plate, respectively, with respect to the modal transverse displacement. The modal in-plane elastic variables U, V, α_x, α_y can be determined from the modal transverse displacement w^0 by using Eq. (17). The reduced subsystem of the plate has the form

$$M^r_{mn}\ddot{w}^0_{mn} + K^r_{mn}w^0_{mn} = q^w_{mn}(t) \tag{20}$$

where the contribution of active electric potentials is incorporated to the vertical surface load.

In the case of the HLPT 3-D, the vector $\bar{\mathbf{u}}_{mn}$ in Eq. (12) contains $9n+3$ elastic variables. The reduction technique is implemented in a similar manner by selecting the top and bottom plate face transverse displacement as independent DOF, thus yielding per mode pair mn two terms for stiffness and mass, respectively, whereas the rest $9n+1$ dependent variables are expressed as a function of top and bottom transverse displacement by means of the Guyan reduction.

2.2. Formulation of plate–impactor structural system

2.2.1. Plate–impactor contact force

In the case of impact of a rigid hard impactor such as steel, on a surface composed of a material of considerably lower stiffness, such as Graphite/Epoxy, the Hertzian contact law (Stronge, 2000) gives rather conservative predictions for the contact force, which develops during impact. Moreover, it leads to increased computational cost due to the non-linear relation between the impact force and the induced local displacement on the impacted face. In the present methodology, linear contact laws have been implemented in order to retain low computational cost and facilitate implementation to real-time control applications. In the case of composite plates, the linear elasto-plastic contact law proposed by Yigit and Christoforou (1994) is implemented. During impact at a point with coordinates (x_0, y_0), the contact force F_i is assumed to vary linearly with the local indentation, which is defined as the relative distance between the impactor position and the face deflection. The latter is assumed to be constant through-thickness in the case of composite plates on the basis of kinematic assumptions (3).

$$F_i(x_0,y_0,t) = \begin{Bmatrix} k_y(w_i(t) - w^0(x_0,y_0,t)), & w_i(t) > w^0(x_0,y_0,t) \\ 0, & w_i(t) \leqslant w^0(x_0,y_0,t) \end{Bmatrix} \tag{21}$$

where w_i is the vertical distance of the impactor (modelled as a point mass) from the plate's surface position just before impact and k_y is the contact stiffness, which depends on impactor radius and elastic properties of impactor and plate material (Christoforou and Yigit, 1998). On the basis of Eq. (21), the simulation of a low-energy impact of a steel sphere on a composite plate includes two distinct impact states: (i) aggregation – plate and impactor motion are coupled and (ii) disaggregation – plate and impactor move independently. The trigger for switching between these two distinct states is the relative distance between impactor position and plate midsurface (Eq. (21)).

In the case of sandwich composite plates, linearized contact laws in the form of Eq. (21) have been adopted, with transverse displacement of the impacted face instead of w^0 and contact stiffness based on either reported values (Anderson, 2005), or values based on the assumption that no damage is induced by the impact event. In the case of damage, the linearized contact law should encompass material degradation effects, such as core crushing, and large face-deflections (Olsson and McManus, 1996; Olsson, 2002), which are not captured by the current methodology. Thus, the values considered herein for the contact stiffness rest on the assumption that no damage takes place throughout the impact event.

A schematic representation of the contact model adopted in the present impact formulation is illustrated in Fig. 2. A fictitious spring with stiffness equal to k_y is assumed to be attached on the midsurface. The impactor is assumed to indent the bottom surface, to attach itself to the spring and to start pushing it upwards, resulting in the development of a plate deflection. After some time, which depends on the values of the initial velocity, plate mass and stiffness, and contact stiffness k_y, the relative velocity between impactor and plate becomes zero (maximum impact force) and the relative distance between plate midsurface – impactor starts to increase up to disaggregation, when the impact force becomes zero. The plate continues to vibrate and, as extensively discussed by Christoforou and Yigit (1998), depending on impact characteristics mentioned above it might even catch up with the impactor and hit it again, yielding a response described as impact chattering (Stronge, 2000).

2.2.2. Plate–impactor structural system

The plate–impactor structural system is formulated by combining the plate subsystem equation (20) with the contact force equation (21), the governing equation of motion of the impactor,

$$m_i\ddot{w}_i(t) = -F_i(x_0,y_0,t) \tag{22}$$

Please cite this article in press as: Plagianakos, T.S., Papadopoulos, E.G. Low-energy impact response of composite and sandwich composite plates with piezoelectric sensory layers. Int. J. Solids Struct. (2014), http://dx.doi.org/10.1016/j.ijsolstr.2014.04.005

and the expression of transverse modal load per unit area q_{mn} by means of Fourier series terms,

$$q_{mn}(x_0,y_0,t)=\frac{4F_i(x_0,y_0,t)}{L_xL_y}\sin\left(\frac{m\pi}{L_x}x_0\right)\sin\left(\frac{n\pi}{L_y}y_0\right) \tag{23}$$

thus describing the governing equations of motion of both impacted plate and impactor:

$$\begin{bmatrix} M^r_{mn} & 0 \\ 0 & m_i \end{bmatrix}\begin{Bmatrix} \ddot{w}^0_{mn}(t) \\ \ddot{w}_i(t) \end{Bmatrix}+\begin{bmatrix} K^r_{mn} & 0 \\ 0 & 0 \end{bmatrix}\begin{Bmatrix} w^0_{mn}(t) \\ w_i(t) \end{Bmatrix} = \begin{Bmatrix} \frac{4k_y\left(w_i(t)-\sum_{i=1}^{\xi}\sum_{j=1}^{\psi}w^0_{ij}(t)\sin\left(\frac{i\pi}{L_x}x_0\right)\sin\left(\frac{j\pi}{L_y}y_0\right)\right)}{L_xL_y}\sin\left(\frac{m\pi}{L_x}x_0\right)\sin\left(\frac{n\pi}{L_y}y_0\right) \\ -k_y\left(w_i(t)-\sum_{i=1}^{\xi}\sum_{j=1}^{\psi}w^0_{ij}(t)\sin\left(\frac{i\pi}{L_x}x_0\right)\sin\left(\frac{j\pi}{L_y}y_0\right)\right) \end{Bmatrix} \quad \begin{matrix} m=1,\ldots,\xi \\ n=1,\ldots,\psi \end{matrix} \tag{24}$$

where ξ, ψ indicate the Fourier modes along x, y, respectively, used to model plate response and transverse load per unit area.

Eq. (24) implies that when the impactor comes into contact with the plate, the ξ and ψ plate vibration modes get excited yielding a relevant contact force, which results to a pressure load analysed to its modal counterparts, each of which is related to the modal transverse deflection by means of Eq. (20). Rearranging Eq. (24) in order to formulate a homogeneous system of differential equations yields the coupled impactor–plate system in time domain:

$$[M_s]\begin{Bmatrix} \ddot{w}^0_{mn}(t) \\ \ddot{w}_i(t) \end{Bmatrix}+[K_s]\begin{Bmatrix} w^0_{mn}(t) \\ w_i(t) \end{Bmatrix}=0 \tag{25}$$

Taking for instance 3×3 modes along the midsurface and assuming impact at the plate's centre, the system mass and stiffness matrices are written as,

$$[M_s]=\begin{bmatrix} M^r_{11} & 0 & 0 & 0 & 0 \\ & M^r_{13} & 0 & 0 & 0 \\ & & M^r_{31} & 0 & 0 \\ & S & & M^r_{33} & 0 \\ & & & & m_i \end{bmatrix} \tag{26}$$

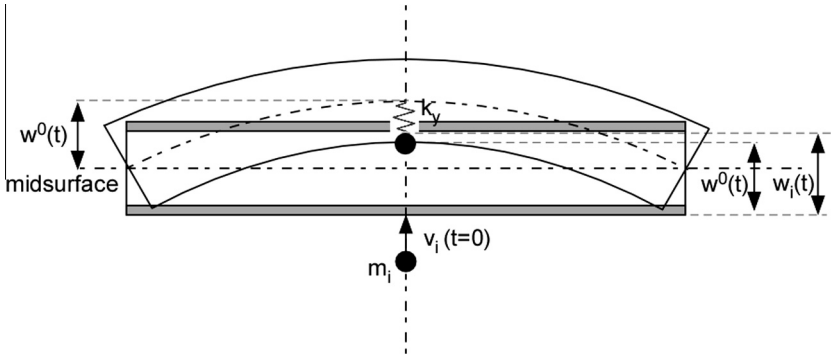

Fig. 2. Schematic representation of the linearized contact model (Yigit and Christoforou, 1994) implemented during impact on a composite plate.

Table 1
Electromechanical properties of materials considered.

Material properties	Composite	Foam	Piezoelectric		
	Gr/Epoxy (Saravanos and Christoforou, 2002a)	Klegecell (Plagianakos and Saravanos, 2009)	PZT-4 (Saravanos and Christoforou, 2002a)	PVDF	PIC 181
Mass density					
ρ (kg/m^3)	1578	45	7600	1780	7800
Elastic properties					
E_{11} (GPa)	120.0	0.035	81.3	3.0	84.7
E_{22} (GPa)	7.9	0.035	81.3	3.0	84.7
E_{33} (GPa)	7.9	0.035	64.5	6.0	70.4
G_{23} (GPa)	5.50	0.0123	25.6	1.0	27.1
G_{13} (GPa)	5.50	0.0123	25.6	1.0	27.1
G_{12} (GPa)	5.50	0.0123	30.6	1.0	31.9
ν_{12}	0.30	0.40	0.33	0.30	0.33
ν_{13}	0.30	0.40	0.43	0.30	0.43
ν_{23}	0.30	0.40	0.43	0.30	0.43
Piezoelectric properties					
d_{31} (10^{-12} m/V)	–	–	−122	−23	−120
d_{32} (10^{-12} m/V)	–	–	−122	−23	−120
d_{33} (10^{-12} m/V)	–	–	285	30	265
d_{36} (10^{-12} m/V)	–	–	0	0	0
d_{15} (10^{-12} m/V)	–	–	495	33	475
d_{24} (10^{-12} m/V)	–	–	495	33	475
Dielectric properties					
ε_{11} (10^{-12} Farad/m)	31	–	13,082	106,000	13,280
ε_{22} (10^{-12} Farad/m)	27	–	13,082	106,000	13,280
ε_{33} (10^{-12} Farad/m)	27	–	11,530	106,000	10,620

Please cite this article in press as: Plagianakos, T.S., Papadopoulos, E.G. Low-energy impact response of composite and sandwich composite plates with piezoelectric sensory layers. Int. J. Solids Struct. (2014), http://dx.doi.org/10.1016/j.ijsolstr.2014.04.005

$$[K_s] = \begin{bmatrix} K^r_{11}+\lambda & -\lambda & -\lambda & \lambda & -\lambda \\ -\lambda & K^r_{13}+\lambda & \lambda & -\lambda & \lambda \\ -\lambda & \lambda & K^r_{31}+\lambda & -\lambda & \lambda \\ \lambda & -\lambda & -\lambda & K^r_{33}+\lambda & -\lambda \\ -k_y & k_y & k_y & -k_y & k_y \end{bmatrix} \tag{27}$$

where $\lambda = 4k_y/(L_xL_y)$.

The system of Eq. (25) is written in state space form as

$$\begin{aligned} \dot{\underset{\sim}{\mathbf{x}}} &= [A]\,\underset{\sim}{\mathbf{x}} \\ \underset{\sim}{\mathbf{y}} &= [C]\,\underset{\sim}{\mathbf{x}} \end{aligned} \tag{28}$$

where $\underset{\sim}{\mathbf{x}}$ and is the vector of state variables,

$$\underset{\sim}{\mathbf{x}} = \{w^0_{mn}, w_i, \dot{w}^0_{mn}, \dot{w}_i\}^T \tag{29}$$

$\underset{\sim}{\mathbf{y}}$ is the vector of output variables, as arising from Eqs. (15) and (11)

$$\underset{\sim}{\mathbf{y}} = \{\overline{\mathbf{u}}_{mn}, w^0_{,x}, w^0_{,y}, \dot{\overline{\mathbf{u}}}_{mn}, \overline{\boldsymbol{\varphi}}^p_{mn}\}^T \tag{30}$$

and $[A]$, $[C]$ are the system and output matrix, respectively:

$$\begin{aligned} [A] &= \begin{bmatrix} 0 & I \\ [M_s]^{-1}[K_s] & 0 \end{bmatrix} \\ [C] &= \begin{bmatrix} \mathbf{T}_{mn} & 0 & 0 & 0 \\ 0 & 0 & \mathbf{T}_{mn} & 0 \\ [K^{PP}_{\varphi\varphi}]^{-1}_{mn}[K^{PP}_{u\varphi}]^T_{mn}\mathbf{T}_{mn} & 0 & 0 & 0 \end{bmatrix} \end{aligned} \tag{31}$$

The slopes of the transverse displacement appearing in Eq. (30) are used for calculating all cubic higher-order displacement terms λ and the quadratic displacement terms of the nth layer (Eq. (3)) by means of the through-thickness interlaminar shear stress compatibility equations (Appendix A). Moreover, an additional physical constraint applied on the electric potential dictates a constant value along the piezoelectric surface, thus a relevant analytical integration is implemented:

$$\overline{\boldsymbol{\varphi}}^p = \frac{4}{\pi^2}\sum_m\sum_n \frac{\overline{\boldsymbol{\varphi}}^p_{mn}}{mn} \tag{32}$$

The state space system of equations (28) is a stiff system due to difference between the plate and contact stiffness value. Therefore, appropriate integration algorithms, such as the Adams-Moulton (ode113 in Matlab) implicit integration scheme with adaptive step-size and convergence tolerance in the range of 1.0e−13, have been implemented.

When the plate loses contact with the impactor ($\lambda = 0$), the equation of motion of the impactor uncouples from the plate structural system (Eq. (25)). The plate vibrates freely with initial conditions the displacement and velocity at the time instant of disaggregation, whereas the impactor is assumed to move with constant velocity, since the acceleration of gravity is negligible compared to the accelerations experienced during an impact.

After solving the structural system of Eq. (28), the displacement and electric potential components are calculated from the respective modal amplitudes (Eq. (30) using Eq. (10) and the interlaminar shear stress compatibility equations (Plagianakos and Saravanos, 2009). Mechanical strain components are calculated by derivation of Eq. (10) and use of interlaminar shear stress compatibility equations, whereas for the electric field, Eq. (2) is implemented. Finally, stresses are calculated by means of the constitutive equations (1). The procedure is similar in the case of the HLPT 3-D, where the modal amplitudes of top and bottom face displacements are the independent DOF included to the structural system and the rest of the elastic and electric variable amplitudes are calculated after solution of the structural system.

3. Results and discussion

The predictions of the current impact mechanics methodology (HLPT 2-D) were validated with predictions of analytical and Ritz-type solutions for composite plates without/with piezoelectric layers (Christoforou and Yigit, 1998; Saravanos and Christoforou, 2002a) and with experimental results for sandwich composite plates reported in the literature (Anderson, 2005). Simply-supported cross-ply plates were studied. The impact took place at the centre of the plates, thus only odd modes were taken into account. The electromechanical properties of materials considered are listed in Table 1.

3.1. Case 1: benchmark composite plate

A $[(0/90)_2/0]_S$ Graphite/Epoxy square composite plate impacted by a steel sphere having a mass of $m_i = 8.537$ g and an initial velocity at contact $v_i = 3.0$ m/s was studied as the first validation case. The plate had an edge length of $a = 0.2$ m and a thickness aspect ratio of $a/h = 74$, whereas each composite ply had a thickness of 0.135 mm. A smeared version of the current higher-order layer-wise theory (actually a higher-order single-layer theory) was used to model the plate through-thickness by applying one discrete

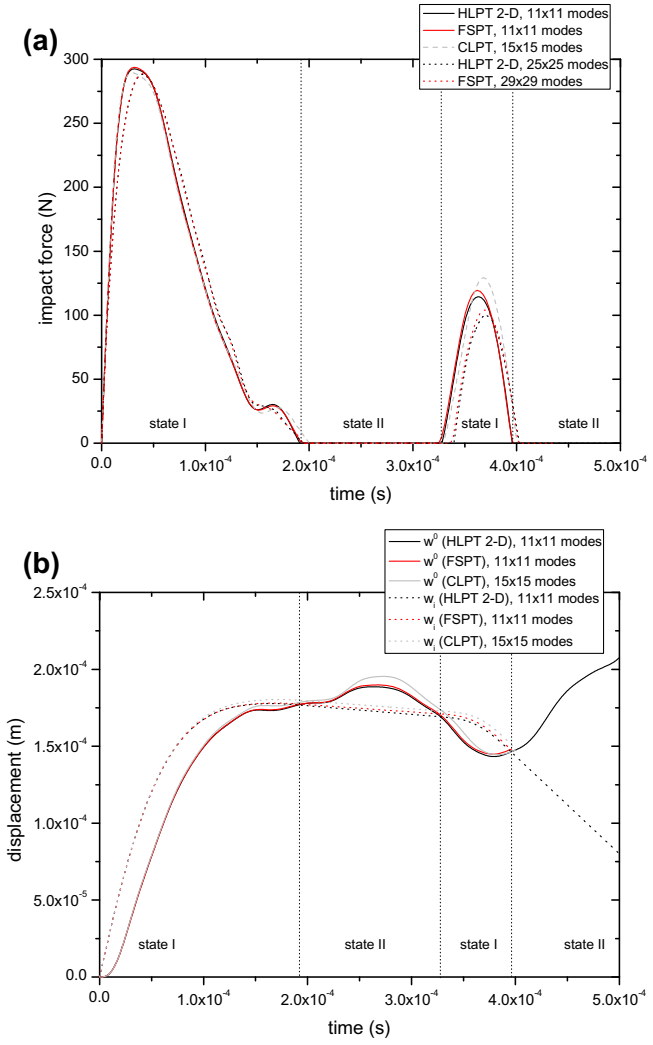

Fig. 3. Validation of current methodology predictions for the case of a small mass impact on a $[(0/90)_2/0]_S$ Gr/Ep plate: (a) impact force, (b) plate displacement and impactor position.

Please cite this article in press as: Plagianakos, T.S., Papadopoulos, E.G. Low-energy impact response of composite and sandwich composite plates with piezoelectric sensory layers. Int. J. Solids Struct. (2014), http://dx.doi.org/10.1016/j.ijsolstr.2014.04.005

Table 2
Predicted natural frequencies of a [pzt-4/(0/90)$_2$/0]$_S$ simply-supported plate using full and reduced higher-order layerwise plate theory (HLPT 2-D).

Mode in x	Mode in y					
	1	3	5	7	9	11
	Natural frequency [kHz]					
Full system						
1	0.4	1.9	4.9	9.1	14.4	20.4
3	2.1	3.4	6.1	10.2	15.4	21.4
5	5.4	6.5	8.9	12.7	17.5	23.3
7	10.1	11.0	13.1	16.4	20.9	26.4
9	15.7	16.6	18.4	21.3	25.3	30.4
11	22.1	23.0	24.7	27.3	30.9	35.6
Reduced system						
1	0.4	1.9	4.9	9.2	14.5	20.7
3	2.1	3.4	6.2	10.3	15.5	21.6
5	5.5	6.5	9.0	12.7	17.7	23.6
7	10.1	11.1	13.2	16.6	21.1	26.7
9	15.8	16.7	18.6	21.6	25.6	30.9
11	22.4	23.2	25.0	27.7	31.3	36.2

layer, since for the thickness aspect ratio and lamination studied, prediction of primary variables as displacement and thus impact force are insensitive to local predictions of interlaminar shear stress at the interface between adjacent layers with different fiber-orientation. The contact stiffness had a value of k_y = 6.65e6 N/m (Christoforou and Yigit, 1998), as arising from yield strength of a typical Graphite/Epoxy composite material (Reese and Bringman, 1978).

Fig. 3 shows predictions of the current methodology for impact force and plate–impactor displacement for a time-window of 0.5 ms, during which the impact is over. The results are validated with those reported using two analytical solutions. The first one is based on first-order shear laminate theory (FSPT) kinematics (Saravanos and Christoforou, 2002a), and takes into account the contribution of the in-plane rotation inertia of the composite laminate to the total plate inertia. The second is based on classical laminate theory (CLPT) kinematics (Christoforou and Yigit, 1998) and neglects such inertia terms. In order to prove convergence, predictions of the current methodology for impact force (Fig. 3(a)) are extracted using 11 × 11 and 25 × 25 Fourier modes, yielding excellent agreement with the FSPT. Note that in the developed method the size of the reduced plate–impactor system was 74 × 74 for 11 × 11 modes, whereas the full system, such as in the case of the FSPT, would have a size of 362 × 362 for equal modes in state space. The required computational time on a dual core processor (3.06 GHz, 6 MB) for the reduced plate impactor system was 1.5% of that of the full system. Thus, the developed method could efficiently capture the wave-controlled impact response of the composite plate (local response occurring prior to reflection of waves from the boundaries, as described by Olsson, 2003), as well as, the impact chattering observed after

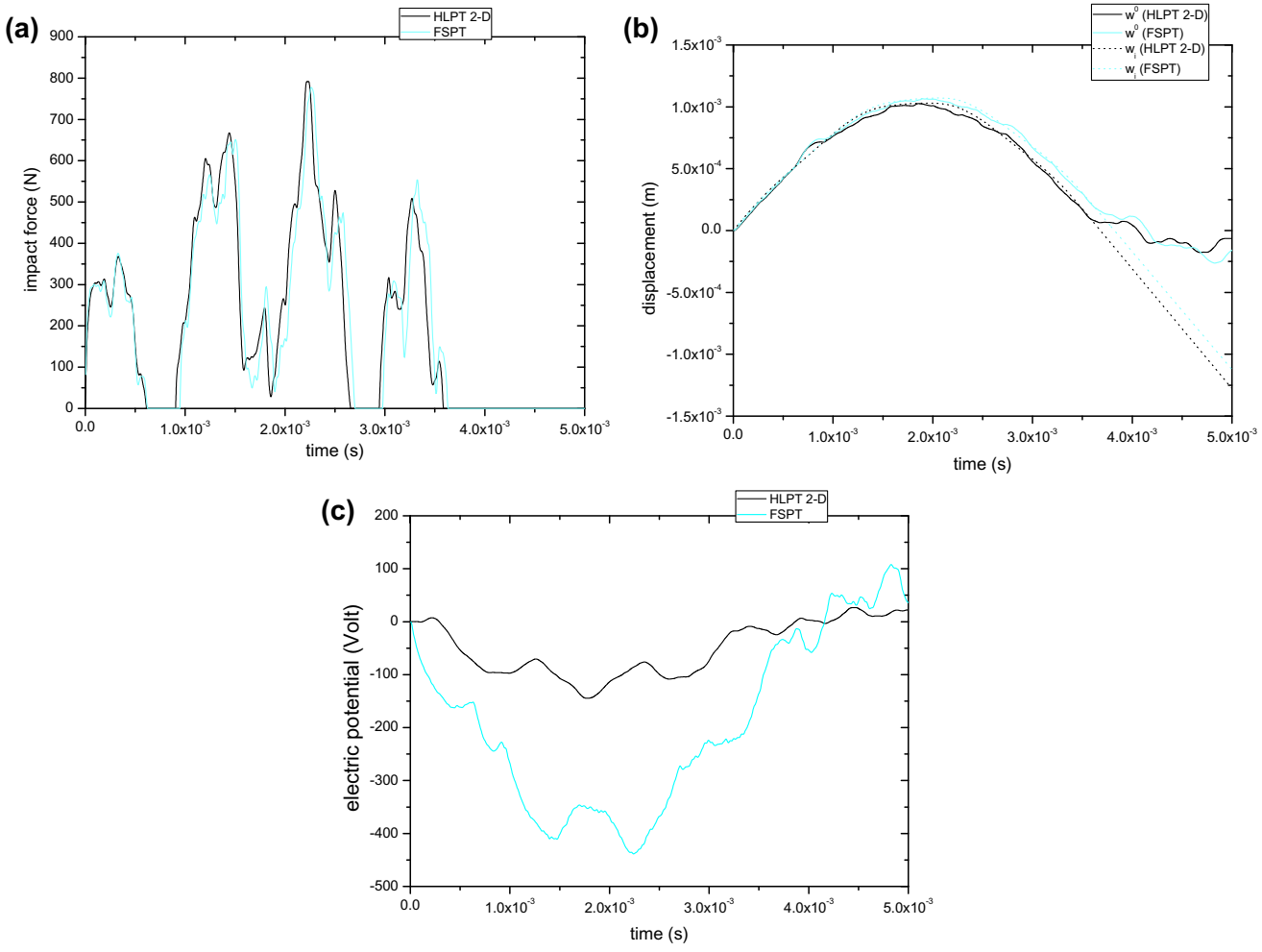

Fig. 4. Validation of current methodology predictions for the case of a 0.5 kg mass impact on a [pzt-4/(0/90)$_2$/0]$_S$ plate: (a) impact force, (b) plate displacement and impactor position, (c) electric potential at lower sensor.

Please cite this article in press as: Plagianakos, T.S., Papadopoulos, E.G. Low-energy impact response of composite and sandwich composite plates with piezoelectric sensory layers. Int. J. Solids Struct. (2014), http://dx.doi.org/10.1016/j.ijsolstr.2014.04.005

t = 0.328 ms. According to Eq. (21), the duration of the two distinct impact states may be determined by the force amplitude, as well as from comparison of predicted displacements for plate and impactor shown in Fig. 3(b).

3.2. Case 2: composite plate with piezoelectric sensory layers

Surface attached sensory piezoelectric layers with inner terminals grounded, having a thickness of 0.25 mm, were added to the composite plate studied above to yield a $[\text{pzt-4}/(0/90)_2/0]_S$ lamination and a thickness aspect ratio a/h = 62.5. The plate was modelled using three discrete layers through thickness, namely one for each piezoelectric layer and one for the composite sublaminate. A contact stiffness k_y = 1.234e7 N/m was assumed (Saravanos and Christoforou, 2002b). Steel spherical impactors with different mass (0.5 and 5.0 kg) were considered in order to indicate response in a transition or a global impact regime (Christoforou and Yigit, 1998), whereas the initial impactor velocity was 1 m/s. The term "global impact" has been borrowed from Christoforou and Yigit (1998) to indicate the quasi-static response dominated by the inertia effects of the impactor, while the plate's vibration is negligible.

In Table 2 the natural frequencies of the plate are presented, which have been calculated by using either the full, or the reduced stiffness and mass matrices of the developed methodology. The full and the reduced system are practically equivalent, since the maximum difference between their predictions is around 1.5%. The

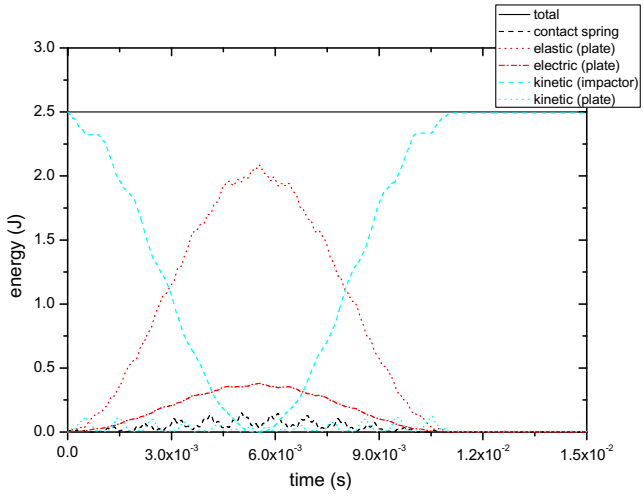

Fig. 6. Energy variation during impact of a 5.0 kg impactor on a $[\text{pzt-4}/(0/90)_2/0]_S$ plate.

impact response of the plate for the case of the medium and large mass impact for 11 × 11 Fourier modes is illustrated in Figs. 4 and 5, respectively. Good agreement is observed between the developed methodology and the analytical solution based on the single-layer FSPT, which implements an explicit integration of

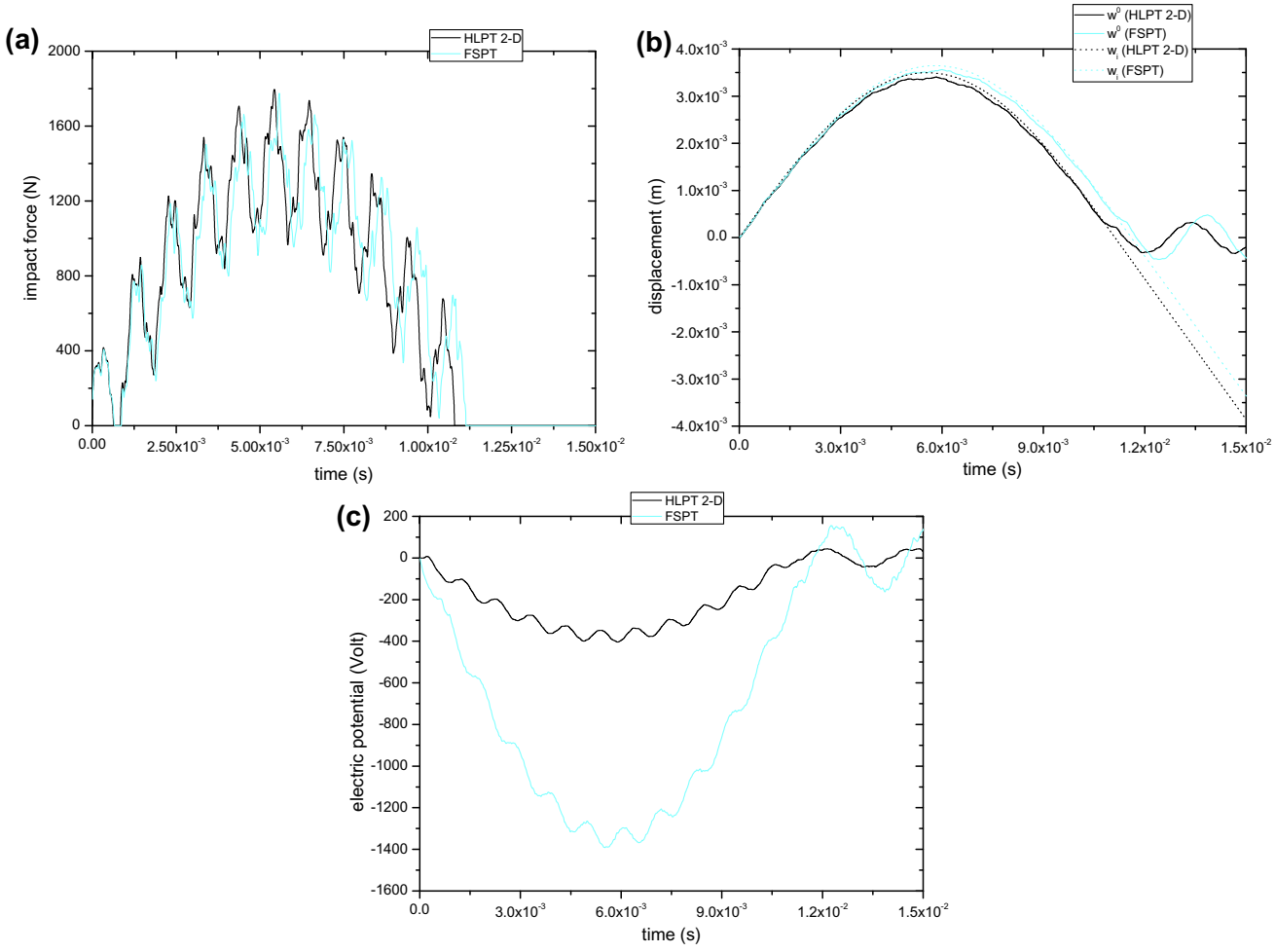

Fig. 5. Validation of current methodology predictions for the case of a 5.0 kg mass impact on a $[\text{pzt-4}/(0/90)_2/0]_S$ plate: (a) impact force, (b) plate displacement and impactor position, (c) electric potential at lower sensor.

Please cite this article in press as: Plagianakos, T.S., Papadopoulos, E.G. Low-energy impact response of composite and sandwich composite plates with piezoelectric sensory layers. Int. J. Solids Struct. (2014), http://dx.doi.org/10.1016/j.ijsolstr.2014.04.005

the full system for impact force, plate displacements and impactor position (Saravanos and Christoforou, 2002a). The predicted variation of the electric potential at the bottom outer face with time for the two impactor masses is illustrated in Figs. 4(c) and 5(c), respectively. The deviations observed between predictions of the current method and FSPT is attributed to the additional in-plane

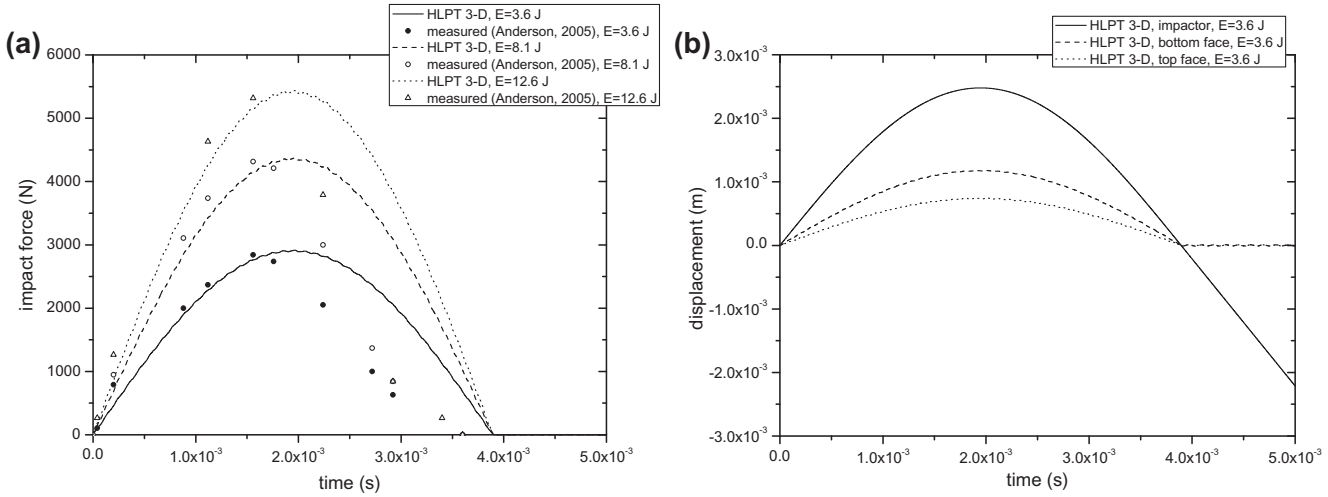

Fig. 7. Validation of current methodology with published measured data for a thick [0/90/0/PMI foam] sandwich composite plate: (a) impact force at three impact energy levels, (b) displacement of impactor and plate's bottom and top face for the lowest energy level. The plate is assumed to be hit upwards on its bottom face.

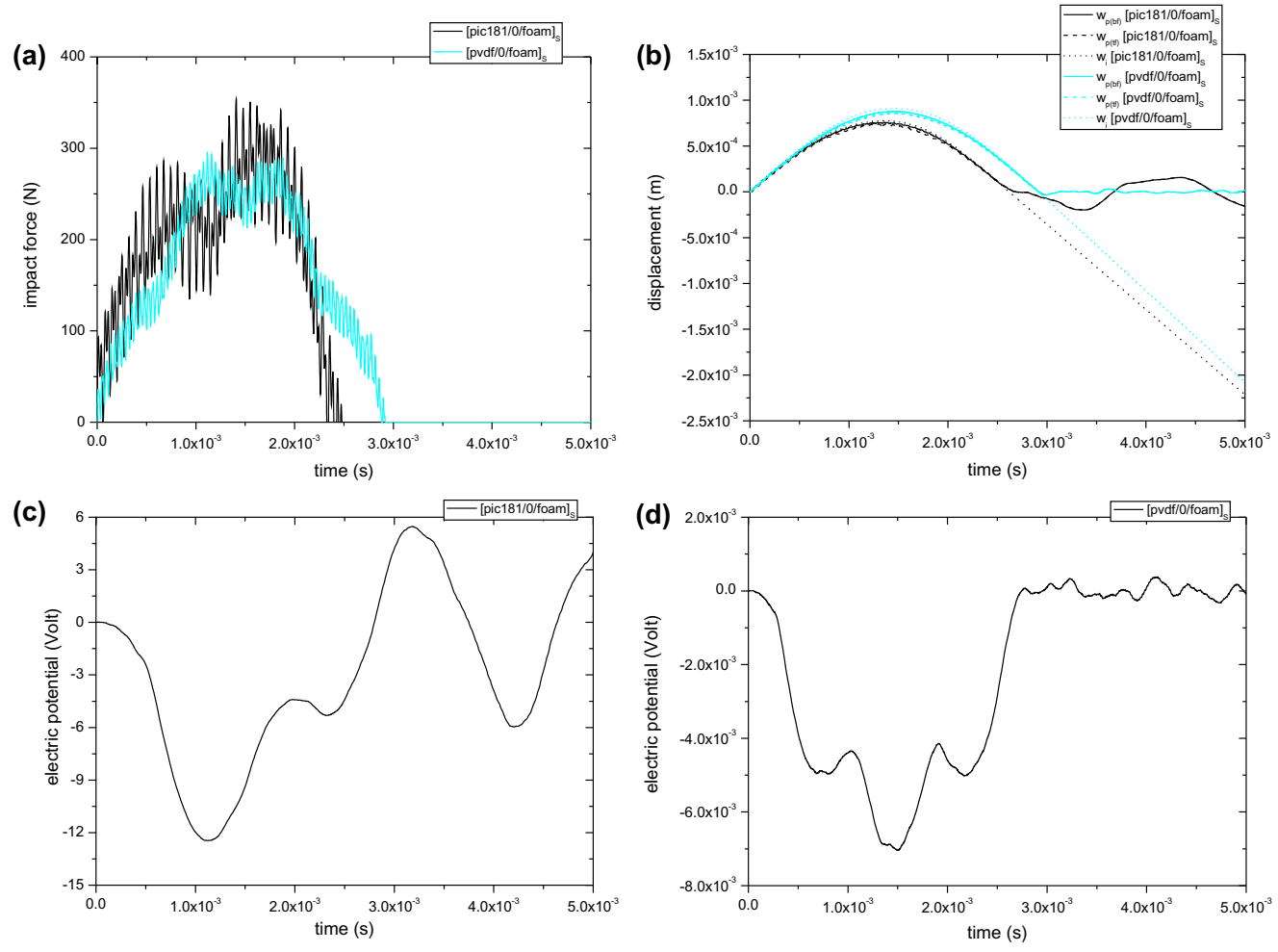

Fig. 8. Impact response of a [pz/0/PVC foam]$_s$ sandwich composite plate for two different piezoelectric materials: (a) impact force, (b) plate displacement and impactor position (bf: bottom face, tf: top face), (c) electric potential at lower outer surface in the case of piezoceramic layers, (d) electric potential at lower outer surface in the case of piezopolymer layers.

Please cite this article in press as: Plagianakos, T.S., Papadopoulos, E.G. Low-energy impact response of composite and sandwich composite plates with piezoelectric sensory layers. Int. J. Solids Struct. (2014), http://dx.doi.org/10.1016/j.ijsolstr.2014.04.005

integration of the electric potential along the *xy*-plane (Eq. (32)). As far as computational effort is concerned, implementation of the developed method, which models the through-thickness response by three discrete layers, led to a plate-impactor system of size 74×74 in state space, as in the previous case study, and to similar computational gain, whereas the solution of a full system of size 938×938 would have been required in the case of no reduction.

In order to quantify the electric energy developed in the piezoelectric layers, which could be used in the case of power autonomous control, the energy equilibrium during impact was studied. Fig. 6 illustrates the temporal variation of potential, kinetic and electric energies developed during impact of the larger mass (5.0 kg) for 3×3 vibration modes. During the loading phase, the kinetic energy of the impactor is gradually transformed to potential energy stored in the fictitious contact spring (Fig. 2), and elastic, electric and kinetic energy in the plate, whereas this process is inversed during the unloading phase. The amount of electric energy developed is considerable in this case, where piezoceramic material layers have been applied. In the case of piezopolymer layers, the electric energy would be negligible, mainly due to lower piezoelectric coefficients.

3.3. Case 3: sandwich composite plate

A simply-supported [0/90/0/foam] thick square sandwich composite plate studied by Anderson (2005) was considered. The plate had an edge length of $a = 0.0762$ m and a thickness aspect ratio of $a/h = 4$, whereas the core consisted of 12.7 mm thick PMI foam. The plate was impacted at its centre by a mass of $m_i = 1.8$ kg, which had an initial velocity of 2, 3 and 3.73 m/s, respectively, resulting in impact energies of 3.6, 8.1 and 12.6 J. The plate was modelled using 3 discrete layers through the thickness and it was impacted upwards on the bottom face. A contact stiffness of $k_y = 2.23\text{e}6$ N/m, reported by Anderson (2005), was assumed and 11×11 Fourier modes were taken into account. Using the HLPT 3-D kinematics of Eq. (3), a reduced structural system of size 146×146 was formulated in state space, including deflection amplitudes of bottom und top face per vibration mode, whereas solution of a system of size 2162×2162 would be required in the case of a full structural system.

Predictions of the HLPT 3-D impact methodology and measured data reported by Anderson (2005) for impact load vs. time for the three different impact energy levels are illustrated in Fig. 7(a). Fairly good agreement between predictions and measurements can be observed for impact force during loading and maximum impact force, whereas the current methodology fails to predict impact force during unloading due to damage effects, such as core crushing, which are neglected in the formulation and the contact law applied. In Fig. 7b the transverse displacement of impactor, bottom face and top face are plotted, illustrating that the current methodology can capture the core compressibility effects occurring during impact.

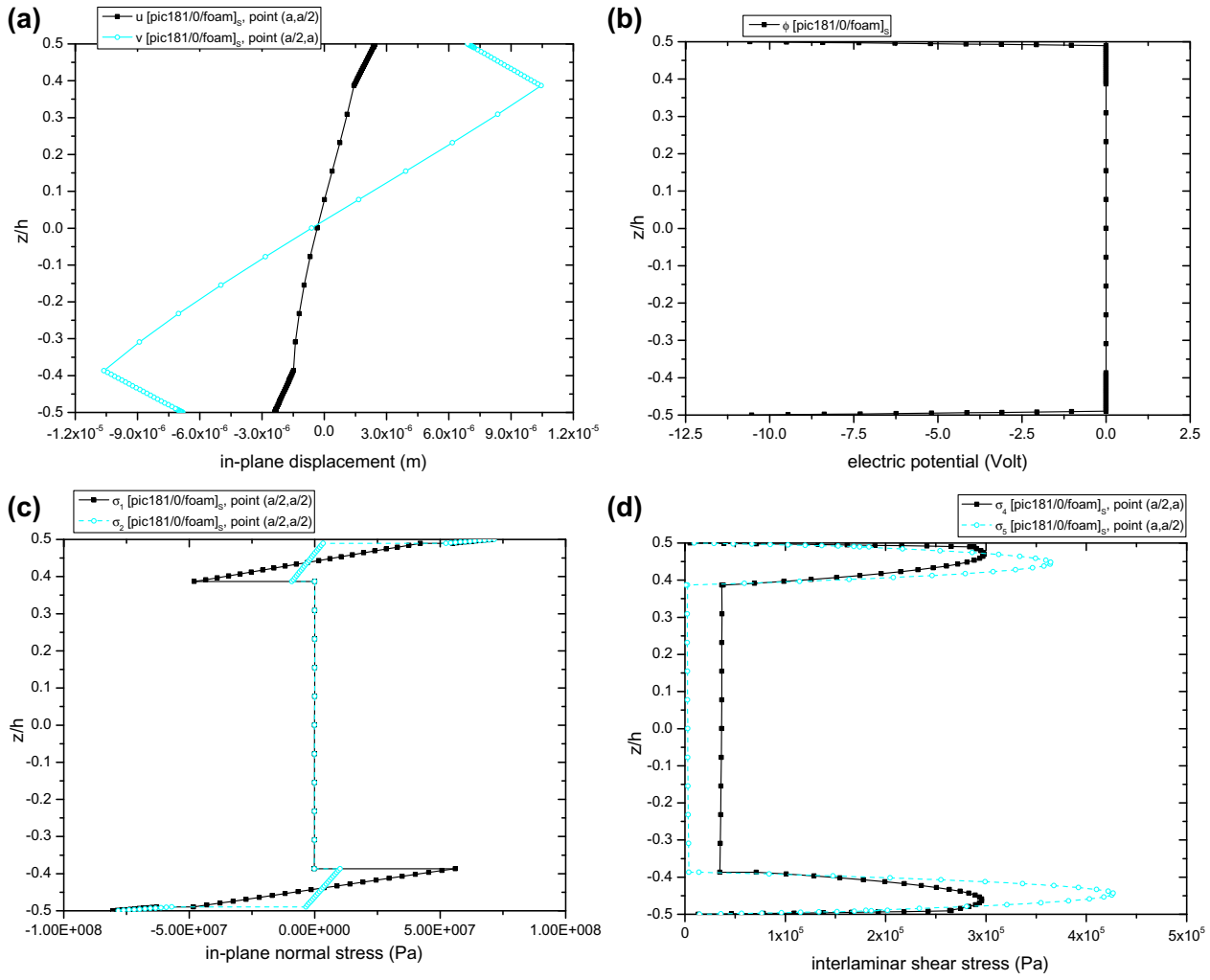

Fig. 9. Through-thickness response of a [pic 181/0/PVC foam]$_s$ sandwich composite plate at points of maximum values and timestep of maximum impact force: (a) in-plane displacements, (b) electric potential, (c) in-plane stresses, (d) interlaminar shear stresses.

Please cite this article in press as: Plagianakos, T.S., Papadopoulos, E.G. Low-energy impact response of composite and sandwich composite plates with piezoelectric sensory layers. Int. J. Solids Struct. (2014), http://dx.doi.org/10.1016/j.ijsolstr.2014.04.005

3.4. Case 4: sandwich composite plate with piezoelectric sensory layers

The impact response of a square $[pz/0/foam]_s$ sandwich composite plate of thickness aspect ratio $a/h = 31$ was studied. The plate consisted of two surface attached piezoelectric layers, each having a thickness of 0.2 mm, Graphite/Epoxy faces of 2 mm each and a 15 mm PVC foam core (Klegecell – DIAB Group). The plate was impacted upwards at the centre of the bottom face by a mass of $m_i = 0.25$ kg having an initial velocity of 1 m/s. To indicate the effect of piezoelectric material on the impact response of the plate, a piezoceramic (PIC 181 – PI Ceramic GmbH) and a piezopolymer (PVDF (DT1-052 K) – MS Inc.) layer were considered. Since no indentation measurements were available, a contact stiffness of 1.234e7 N/m (Saravanos and Christoforou, 2002b) and 7.0e6 N/m were assumed for the piezoceramic and piezopolymer material, respectively, on the basis that no damage takes place. Both contact stiffness values are in the range of linearized Hertzian contact for the predicted indentations. The plate was modelled using five discrete layers through-thickness, namely one for each material sublaminate, resulting to 46 deflection-dependent DOF per mode. In this case, 15×15 modes were used for predicting the impact response of the plate, resulting to the formulation of a reduced structural system of size 258×258 in state-space, whereas solution of a system of size 6146×6146 would be required in the case of a full structural system.

Fig. 8 illustrates the impact response of the plate in the case of piezoceramic and piezopolymer sensory layers. The piezoelectric material strongly affects the impact force, mainly due to the value of contact stiffness. As seen in Fig. 8(a) there is practically a single impact event for both piezoceramic and piezopolymer layers and force and deflection, shown in Fig. 8(b) are in-phase. Thus, for both piezoelectric materials a rather global impact response may be observed. In realistic control applications, the type and duration of impact and the electric energy developed are of major importance, since they determine the feasibility of control during the impact event. As expected, the maximum impact force is much higher, and impact duration much shorter in the case of the piezoceramic layer due to a higher contact stiffness. As far as the conversion of the kinetic to electric energy is concerned, the piezoceramic layer is much more efficient, as indicated by the temporal variation of the electric potential presented in Fig. 8(c) and (d) for these piezoelectric materials, respectively. The large difference between the two piezoelectric materials in impact-induced electric potential is attributed to both electromechanical properties and contact stiffness. The fact that the piezoelectric coefficients of the piezoceramic material are higher than those of the piezopolymer, combined with the higher contact stiffness, lead to higher strains and higher conversion of mechanical to electric energy in the piezoelectric layer, as mandated by the constitutive equation (1).

Fig. 9 shows the predicted electromechanical local through-thickness response at points of maximum values at the timestep corresponding to maximum impact force. Fig. 9(a)–(d) highlight

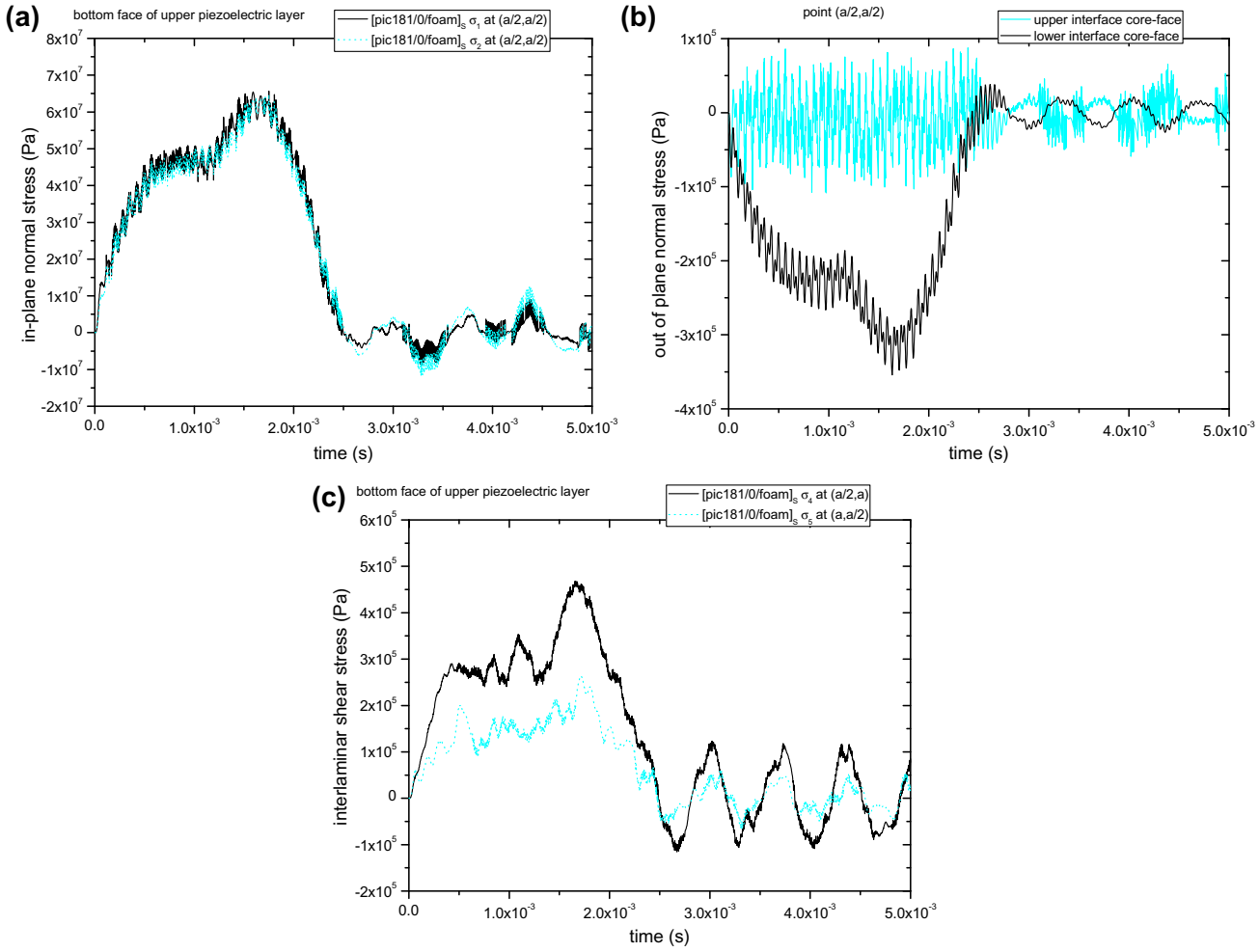

Fig. 10. Variation of stress at interfaces between different material layers with time at points of maximum values in a [pic 181/0/PVC foam]$_s$ sandwich composite plate: (a) in-plane stresses at interface between composite-piezoelectric material layer, (b) out of plane normal stress at the interfaces between core and faces, (c) interlaminar shear stresses at interface between composite-piezoelectric material layer.

Please cite this article in press as: Plagianakos, T.S., Papadopoulos, E.G. Low-energy impact response of composite and sandwich composite plates with piezoelectric sensory layers. Int. J. Solids Struct. (2014), http://dx.doi.org/10.1016/j.ijsolstr.2014.04.005

the benefit of implementing higher-order layerwise kinematic assumptions, since piecewise through-thickness distributions up to second order can be efficiently captured using a minimum number of discrete layers. Especially in the case of interlaminar shear stress (Fig. 9(d)) the developed methodology efficiently captures parabolic through-thickness distributions at the sandwich faces using five discrete layers through the thickness of the laminate. The latter is a major advantage compared to linear layerwise laminate theories, which would require a large number of discrete layers and thus degrees of freedom in order to capture such through-thickness stress profiles (Plagianakos and Saravanos, 2008, 2009). On the other hand, the lack of explicit imposition of shear stress compatibility equations leads to non-zero interlaminar shear stresses at the free faces, although they tend to get to zero. The enhanced capabilities of the developed methodology regarding efficiency include information concerning the through-thickness response during impact and prediction of stress at adjacent material interfaces, while the size of structural matrices participating to the solution after the impact event is kept small by expressing all structural parameters as a function of modal deflection amplitudes, as described in Section 2.1.7. Prediction of the temporal stress variation at a particular point of interest is useful for having an idea of the possibility of damage initiation in the form of core crushing, delamination and matrix cracks, and design accordingly. Fig. 10 illustrates such a prediction of stress tensor components at the interface between different material layers. In Fig. 10(a) and (c), in-plane normal and interlaminar shear stresses at the interface between composite-piezoelectric layer are plotted. The latter prediction is useful in order to estimate probable delamination of the piezoelectric layer. Fig. 10 shows predicted temporal variation of the out of plane normal stress at the interfaces between composite faces and foam core. Taking into account the failure criterion of Besant et al. (2001) and the foam strength data (compressive strength 0.5 MPa, shear strength 0.6 MPa), it can be observed that the foam does not fail.

The proposed methodology can predict the stress field developed in a composite or a sandwich composite plate with piezoelectric layers subjected to low-energy impact, while remaining within the limits of linear elastic response. It has been developed for use in real-time control applications, where the amount of state variables and the size of the system matrices are of major importance. The initiation of damage is combined with non-linear phenomena that are not captured. If extended to account for non-linear effects, such as large displacements and material degradation, it will be able to predict damage initiation and propagation; this can be the subject of future work.

4. Summary

A novel model-reduction based methodology for predicting both global and local low-energy impact response of pristine simply-supported cross-ply composite and sandwich composite plates with piezoelectric sensory layers was presented. The methodology combines novel higher-order layerwise through-thickness kinematics, which account for core transverse compressibility, and a Guan reduction technique. Its major advantage over single-layer or linear layerwise analytical solutions or finite element formulations lies in the computational efficiency, which leads to at least an 80% saving in system size and thus leads to comparable reduction in computational effort, whereas it predicts stresses at interfaces between different material layers. Contributions of the paper include prediction of the low-energy impact response of sandwich composite plates with piezoelectric layers, quantification of the effect of piezoelectric material on the global impact response (impact force, displacement and electric potential) and prediction of the electric energy developed in the piezoelectric layers during impact on composite plates. The developed methodology leads to formulation of low-size systems in state space, thus facilitating applicability in real-time impact and vibration control, which will be topics of research to follow.

Acknowledgments

The research leading to the results presented in this work has received funding from the People Programme (Marie Curie Actions) of the European Unions' Seventh Framework Programme (FP7/2007-2013) under REA Grant agreement No. 299089.

Appendix A

A.1. Composite ply tensors (HLPT 2-D)

The stiffness tensor of a unidirectional orthotropic composite ply is formulated in the material coordinate system as follows:

$$[\mathbf{Q}_l] = \begin{bmatrix} Q_{l11} & Q_{l12} & 0 & 0 & 0 \\ & Q_{l22} & 0 & 0 & 0 \\ & & Q_{l44} & 0 & 0 \\ & S & & Q_{l55} & 0 \\ & & & & Q_{l66} \end{bmatrix} \tag{A1}$$

where S denotes symmetry and the matrix terms are given by:

$$Q_{l11} = \frac{E_{11}}{1 - v_{12}v_{21}}, \quad Q_{l12} = \frac{v_{12}E_{11}}{1 - v_{12}v_{21}},$$
$$Q_{l22} = \frac{E_{22}}{1 - v_{12}v_{21}}, \quad Q_{l44} = G_{23}, \quad Q_{l55} = G_{13}, \quad Q_{l66} = G_{12} \tag{A2}$$

The off-axis stiffness matrix of a ply having fibers aligned at an angle θ to the natural coordinate system is derived by the rotational transformation for second-order tensors:

$$[\mathbf{Q}_c] = [\mathbf{R}]^{-1}[\mathbf{Q}_l][\mathbf{R}]^{-T} \tag{A3}$$

where $[\mathbf{R}]$ is the rotational transformation matrix:

$$[\mathbf{R}] = \begin{bmatrix} m^2 & n^2 & 0 & 0 & 2mn \\ n^2 & m^2 & 0 & 0 & -2mn \\ 0 & 0 & m & -n & 0 \\ 0 & 0 & n & m & m \\ -mn & mn & 0 & 0 & m^2 - n^2 \end{bmatrix} \text{ with } m = \cos\theta \text{ and } n = \sin\theta \tag{A4}$$

A.2. Piezoelectric ply tensors (HLPT 2-D)

The piezoelectric charge tensor has the following form:

$$[d_l] = \begin{bmatrix} 0 & 0 & 0 & d_{15} & 0 \\ 0 & 0 & d_{24} & 0 & 0 \\ d_{31} & d_{32} & 0 & 0 & 0 \end{bmatrix} \tag{A5}$$

The piezoelectric tensor $[e_l]$ appearing in the constitutive Eq. (1) is formulated from the piezoelectric charge tensor and the stiffness tensor as follows:

$$[e_l] = [d_l][C_l] \tag{A6}$$

A.3. Through-thickness polynomial functions

The polynomial functions developed for the approximation of in-plane displacements and electric potential through the thickness of each discrete layer are:

Please cite this article in press as: Plagianakos, T.S., Papadopoulos, E.G. Low-energy impact response of composite and sandwich composite plates with piezoelectric sensory layers. Int. J. Solids Struct. (2014), http://dx.doi.org/10.1016/j.ijsolstr.2014.04.005

$$\Psi_1^k = (1-\zeta_k)/2$$
$$\Psi_2^k = (1+\zeta_k)/2$$
$$\Psi_3^k = \frac{h_k}{2}(\zeta_k^2 - 1) \tag{A7}$$
$$\Psi_4^k = \frac{h_k}{2}\zeta_k(\zeta_k^2 - 1)$$

In the above equation ζ_k is the local thickness coordinate of layer k, given by:

$$\zeta_k = \frac{2}{h_k}z - \frac{z_1^k + z_2^k}{h_k} \tag{A8}$$

where h_k is the thickness of the discrete layer and z_1^k, z_2^k are the z-axis coordinates of the bottom and top surfaces of the kth discrete layer, respectively (Fig. 1(a)).

A.4. Discrete layer strain vectors

On the basis of the kinematic assumptions (3), the full strain vectors appearing in Eq. (5) in the case of the HLPT 2-D are formulated as,

$$S_1^k = U_{,x}^k\Psi_1^k + U_{,x}^{k+1}\Psi_2^k + \alpha_{x,x}^k\Psi_3^k + \lambda_{x,x}^k\Psi_4^k$$
$$S_2^k = V_{,y}^k\Psi_1^k + V_{,y}^{k+1}\Psi_2^k + \alpha_{y,y}^k\Psi_3^k + \lambda_{y,y}^k\Psi_4^k$$
$$S_{6a}^k = U_{,y}^k\Psi_1^k + U_{,y}^{k+1}\Psi_2^k + \alpha_{x,y}^k\Psi_3^k + \lambda_{x,y}^k\Psi_4^k$$
$$S_{6b}^k = V_{,x}^k\Psi_1^k + V_{,x}^{k+1}\Psi_2^k + \alpha_{y,x}^k\Psi_3^k + \lambda_{y,x}^k\Psi_4^k \tag{A9}$$
$$S_4^k = w_{,y}^0 + \frac{V^{k+1} - V^k}{h_k} + 2\zeta_k\alpha_y^k + (3\zeta_k^2 - 1)\lambda_y^k$$
$$S_5^k = w_{,x}^0 + \frac{U^{k+1} - U^k}{h_k} + 2\zeta_k\alpha_x^k + (3\zeta_k^2 - 1)\lambda_x^k$$

A.5. Interlaminar shear stress compatibility

In a sandwich piezoelectric composite laminate modelled with n-discrete layers through-thickness interlaminar shear stresses should be continuous between discrete layers and vanish at top and bottom of the laminate:

$$\begin{aligned} &\sigma_4^1(\zeta_1 = -1) = \sigma_5^1(\zeta_1 = -1) = 0 && (a)\\ &\sigma_4^k(\zeta_k = 1) = \sigma_4^{k+1}(\zeta_{k+1} = -1) && \\ &\sigma_5^k(\zeta_k = 1) = \sigma_5^{k+1}(\zeta_{k+1} = -1) \quad k = 1,\ldots,n-1 && (b)\\ &\sigma_4^n(\zeta_n = 1) = \sigma_5^n(\zeta_n = 1) = 0 && (c) \end{aligned} \tag{A10}$$

By taking into account the constitutive equation (1) and discrete layers strains of Eq. (A9) the above equations are rearranged as:

$$\begin{Bmatrix}\lambda_y^k\\ \lambda_x^k\end{Bmatrix} = [\tilde{\Lambda}^{(k,k)}]\Xi_s^k + [\tilde{\Lambda}^{(k,k-1)}]\Xi_s^{k-1} + \cdots + [\tilde{\Lambda}^{(k,1)}]\Xi_s^1 \qquad (a)$$

$$\begin{Bmatrix}\alpha_y^n\\ \alpha_x^n\end{Bmatrix} = [\hat{\Lambda}^{(n,n)}]\begin{Bmatrix}\Xi_s^{*n}\\ \lambda_y^n\\ \lambda_x^n\end{Bmatrix} \qquad (b) \tag{A11}$$

$$\begin{Bmatrix}\lambda_y^n\\ \lambda_x^n\end{Bmatrix} = [\tilde{\Lambda}^{*(n,n)}]\Xi_s^{*n} + [\tilde{\Lambda}^{(n,n-1)}]\Xi_s^{n-1} + \cdots + [\tilde{\Lambda}^{(n,1)}]\Xi_s^1 \qquad (c)$$

where $\tilde{\Lambda}$, $\hat{\Lambda}$ and $\tilde{\Lambda}^*$ are reduction matrices and their superscript denotes expression of higher-order terms of layer k as a function of terms of that layer and all layers below (Plagianakos and Saravanos, 2009) included in vectors,

$$\Xi_s^k = \left\{w_{,y}^o, V^k, V^{k+1}, w_{,x}^o, U^k, U^{k+1}, \alpha_y^k, \alpha_x^k\right\}$$
$$\Xi_s^{*n} = \left\{w_{,y}^o, V^n, V^{n+1}, w_{,x}^o, U^n, U^{n+1}\right\} \tag{A12}$$

Derivation of Eq. (A11) with respect to x, y yields higher-order terms participating in the expression of discrete layer in-plane strains. Imposition of the interlaminar shear stress compatibility conditions of Eq. (A11) on the discrete layer stiffness matrices yields the reduced vectors $\boldsymbol{S}_s$ and $\boldsymbol{S}_s^k$ of Eq. (7), explicitly given in Eq. (9).

References

Abrate, S., 1997. Localized impact on sandwich structures with laminated facings. Appl. Mech. Rev. 50, 69–82.
Abrate, S., 1998. Impact on Composite Structures. Cambridge University Press.
Abrate, S., 2001. Modeling of impacts on composite structures. Compos. Struct. 51, 129–138.
Ambur, D.R., Prasad, C.B., Waters, W.A., 1995. A dropped-weight apparatus for low-speed impact testing of composite structures. Exp. Mech. 35, 77–82.
Anderson, T.A., 2005. An investigation of SDOF models for large mass impact on sandwich composites. Compos. B 36, 135–142.
Avitabile, P., 2005. Model reduction and model expansion and their applications Part 1 theory. In: Proc. 23rd Int. Modal Analysis Conf., Orlando, FL, US.
Besant, T., Davies, G.A.O., Hitchings, D., 2001. Finite element modelling of low velocity impact of composite sandwich panels. Compos. A 32, 1189–1196.
Cantwell, W.J., Morton, J., 1991. The impact resistance of composite materials – a review. Composites 22, 347–362.
Chai, G.B., Zhu, S., 2011. A review of low-velocity impact on sandwich structures. J. Mater. Des. Appl. 225, 207–230.
Choi, H.Y., Chang, F.K., 1992. A model for predicting damage in graphite/epoxy laminated composites resulting from low-velocity point impact. J. Compos. Mater. 26, 2134–2169.
Christoforou, A.P., Swanson, S.R., 1991. Analysis of impact response in composite plates. Int. J. Solids Struct. 27, 161–170.
Christoforou, A.P., Yigit, A.S., 1998. Characterization of impact in composite plates. Compos. Struct. 43, 15–24.
Christoforou, A.P., Yigit, A.S., Cantwell, W.J., Yang, F., 2010. Impact response characterization in composite plates – experimental validation. Appl. Compos. Mater. 17, 463–472.
Chun, L., Lam, K.Y., 1998. Dynamic response of fully-clamped laminated composite plates subjected to low-velocity impact of a mass. Int. J. Solids Struct. 35, 963–979.
Guyan, R.J., 1965. Reduction of stiffness and mass matrices. AIAA J. 3, 380-380.
Hazizan, M.A., Cantwell, W.J., 2002. The low velocity impact response of foam-based sandwich structures. Compos. B 33, 193–204.
Hoo Fatt, M.S., Park, K.S., 2001. Dynamic models for low-velocity impact damage of composite sandwich panels – Part A: deformation. Compos. Struct. 52, 335–351.
Icardi, U., Ferrero, L., 2009. Impact analysis of sandwich composites based on a refined plate element with strain energy updating. Compos. Struct. 89, 35–51.
Kärger, L., Baaran, J., Tessmer, J., 2008. Efficient simulations of low-velocity impacts on composite sandwich panels. Comput. Struct. 86, 988–996.
Lee, L.J., Huang, K.Y., Fann, Y.J., 1993. Dynamic responses of composite sandwich plate impacted by a rigid ball. J. Compos. Mater. 27, 1238–1256.
Liu, Y., Chattopadhyay, A., 2013. Low-velocity impact damage monitoring of a sandwich composite wing. J. Intell. Mater. Sys. Struct. 24, 2074–2083.
Malekzadeh, K., Khalili, M.R., Olsson, R., Jafari, A., 2006. Higher-order dynamic response of composite sandwich panels with flexible core under simultaneous low-velocity impacts of multiple small masses. Int. J. Solids Struct. 43, 6667–6687.
Olsson, R., 2002. Engineering method for prediction of impact response and damage in sandwich panels. J. Sandw. Struct. Mater. 4, 3–29.
Olsson, R., 2003. Closed form prediction of peak load and delamination onset under small mass impact. Compos. Struct. 59, 341–349.
Olsson, R., McManus, H.L., 1996. Improved theory for contact indentation of sandwich panels. AIAA J. 34, 1238–1244.
Palazotto, A.N., Herup, E.J., Gummadi, L.N.B., 2000. Finite element analysis of low-velocity impact on composite sandwich plates. Compos. Struct. 49, 209–227.
Park, J., Ha, S., Chang, F.K., 2009. Monitoring impact events using a system-identification method. AIAA J. 47, 2011–2021.
Plagianakos, T.S., Saravanos, D.A., 2008. Coupled high-order layerwise laminate theory for sandwich composite plates with piezoelectric actuators and sensors. In: Proc. 19th Int. Conf. Adaptive Struct. Technol. (ICAST), Ascona CH.
Plagianakos, T.S., Saravanos, D.A., 2009. High-order layerwise finite element for the damped free-vibration response of thick composite and sandwich composite plates. Int. J. Numer. Methods Eng. 77, 1593–1626.
Qiu, X.M., Yu, T.X., 2011. Some topics in recent advances and applications of structural impact dynamics. Appl. Mech. Rev. 64, 12 pages.
Qu, Z.Q., 2004. Model Order Reduction Techniques with Applications in Finite Element Analysis. Springer, London.
Reese, C., Bringman, P., 1978. Determination of shear strength distributions for graphite-epoxy composite materials. Annu. Rep. NASA Grant NSG 1281.
Saravanos, D.A., Christoforou, A.P., 2002a. Impact response of adaptive piezoelectric laminated plates. AIAA J. 40, 2087–2095.
Saravanos, D.A., Christoforou, A.P., 2002b. Low-energy impact of adaptive cylindrical piezoelectric-composite shells. Int. J. Solids Struct. 39, 2257–2279.
Saravanos, D.A., Heyliger, P.R., 1995. Coupled layerwise analysis of composite beams with embedded piezoelectric sensors and actuators. J. Intell. Mater. Sys. Struct. 6, 350–363.

Please cite this article in press as: Plagianakos, T.S., Papadopoulos, E.G. Low-energy impact response of composite and sandwich composite plates with piezoelectric sensory layers. Int. J. Solids Struct. (2014), http://dx.doi.org/10.1016/j.ijsolstr.2014.04.005

Schubel, P.M., Luo, J.J., Daniel, I.M., 2005. Low velocity impact behaviour of composite sandwich panels. Compos. A 36, 1389–1396.
Seydel, R., Chang, F.K., 2001. Impact identification of stiffened composite panels: I. System development. Smart Mater. Struct. 10, 354–369.
Shivakumar, K.N., Elber, W., Illg, W., 1985. Prediction of impact force and duration due to low-velocity impact on circular composite laminates. J. Appl. Mech. 52, 674–680.
Sjöblom, P.O., Hartness, J.T., Cordell, T.M., 1988. On low-velocity impact testing of composite materials. J. Compos. Mater. 22, 30–52.
Stronge, W.J., 2000. Impact Mechanics. Cambridge University Press.
Sun, C.T., Chen, J.K., 1985. On the impact of initially stressed composite laminates. J. Compos. Mater. 19, 490–504.
Tracy, M., Chang, F.K., 1998. Identifying impacts in composite plates with piezoelectric strain sensors, Part I: theory. J. Intell. Mater. Sys. Struct. 9, 920–928.
Wu, H.Y.T., Chang, F.K., 1989. Transient dynamic analysis of laminated composite plates subjected to transverse impact. Comput. Struct. 31, 453–466.
Wu, K.Q., Yu, T.X., 2001. Simple dynamic models of elasto-plastic structures under impact. Int. J. Impact Eng. 25, 735–754.
Yang, M., Qiao, P., 2005. Higher-order impact modelling of sandwich structures with flexible core. Int. J. Solids Struct. 42, 5460–5490.
Yang, F.J., Hassan, M.Z., Cantwell, W.J., Jones, N., 2013. Scaling effects in the low velocity impact response of sandwich structures. Compos. Struct. 99, 97–104.
Yigit, A.S., Christoforou, A.P., 1994. On the impact of a spherical indenter and an elastic–plastic transversely isotropic half-space. Compos. Eng. 4, 1143–1152.
Zhou, D.W., Stronge, W.J., 2006. Low-velocity impact denting of HSSA lightweight sandwich panel. Int. J. Mech. Sci. 48, 1031–1045.

Please cite this article in press as: Plagianakos, T.S., Papadopoulos, E.G. Low-energy impact response of composite and sandwich composite plates with piezoelectric sensory layers. Int. J. Solids Struct. (2014), http://dx.doi.org/10.1016/j.ijsolstr.2014.04.005